Infectious Disease Modelling 6 (2021) 1–21

Contents lists available at ScienceDirect

Infectious Disease Modelling

journal homepage: www.keaipublishing.com/idm

A primer on using mathematics to understand COVID-19 dynamics: Modeling, analysis and simulations

Abba B. Gumel [a, e, *], Enahoro A. Iboi [b], Calistus N. Ngonghala [c, d], Elamin H. Elbasha [f]

[a] School of Mathematical and Statistical Sciences, Arizona State University, Tempe, AZ, 85287, USA
[b] Department of Mathematics, Spelman College, Atlanta, GA, 30314, USA
[c] Department of Mathematics, University of Florida, Gainesville, FL, 32611, USA
[d] Emerging Pathogens Institute, University of Florida, Gainesville, FL, 32610, USA
[e] Department of Mathematics and Applied Mathematics, University of Pretoria, Pretoria, 0002, South Africa
[f] Merck & Co., Inc., 2000 Galloping Hill Road, Kenilworth, NJ, 07033, USA

ARTICLE INFO

Article history:
Received 15 September 2020
Received in revised form 11 November 2020
Accepted 14 November 2020
Available online 30 November 2020
Handling Editor: Dr. J Wu

Keywords:
COVID-19
SARS-CoV-2
Non-pharmaceutical interventions
Face mask
Reproduction number

ABSTRACT

The novel coronavirus (COVID-19) pandemic that emerged from Wuhan city in December 2019 overwhelmed health systems and paralyzed economies around the world. It became the most important public health challenge facing mankind since the 1918 Spanish flu pandemic. Various theoretical and empirical approaches have been designed and used to gain insight into the transmission dynamics and control of the pandemic. This study presents a primer for formulating, analysing and simulating mathematical models for understanding the dynamics of COVID-19. Specifically, we introduce simple compartmental, Kermack-McKendrick-type epidemic models with homogeneously- and heterogeneously-mixed populations, an endemic model for assessing the potential population-level impact of a hypothetical COVID-19 vaccine. We illustrate how some basic non-pharmaceutical interventions against COVID-19 can be incorporated into the epidemic model. A brief overview of other kinds of models that have been used to study the dynamics of COVID-19, such as agent-based, network and statistical models, is also presented. Possible extensions of the basic model, as well as open challenges associated with the formulation and theoretical analysis of models for COVID-19 dynamics, are suggested.

1. Introduction

A novel coronavirus emerged out of Wuhan city of China in December of 2019. The disease (appropriately coined COVID-19, to indicate that it is a member of the coronavirus family of viruses identified in the year 2019) started as an outbreak of pneumonia of unknown cause. It rapidly became a devastating pandemic, spreading to every country on earth, and inflicting severe public health and socio-economic burden globally (Branswell, 2020). By the end of August 2020, the pandemic caused

* Corresponding author. School of Mathematical and Statistical Sciences, Arizona State University, Tempe, AZ, 85287, USA.
E-mail address: agumel@asu.edu (A.B. Gumel).
Peer review under responsibility of KeAi Communications Co., Ltd.

https://doi.org/10.1016/j.idm.2020.11.005

over 25.6 million confirmed cases and 854, 000 deaths globally. China was the first epicenter of COVID-19, followed by Europe (with Italy and the United Kingdom bearing the brunt of the burden), then the US (Dong, Du, & Gardner, 2020). The United States (US) recorded its first documented COVID-19 confirmed case on January 20, 2020. This was linked to a resident who returned from a trip to Wuhan city. By August 31, 2020, the US has recorded over 6 million confirmed cases and 187, 700 deaths. Although recent modeling data showed that COVID-19 was already spreading in the State of New York by late January 2020 (Ngonghala et al., 2020a), the officially reported "index case" for the State was documented on March 1, 2020 (which was traced to a woman who traveled to New York city from Iran, a country that was ravaged by COVID-19 at that time). Starting with the official "index case" on March 1, 2020, the State of New York recorded nearly 70, 000 confirmed cases and about 1, 000 deaths by the end of March 2020. These numbers skyrocketed to over 300, 000 cases and 17, 000 deaths, respectively, by the end of April 2020, illustrating early exponential growth of the pandemic (Dong et al., 2020).

COVID-19 is transmitted from human-to-human through direct contact with contaminated objects or surfaces and through inhalation of respiratory droplets from both symptomatic and -infectious humans. There is also limited evidence that the virus can be exhaled through normal breathing. The incubation period of COVID-19 ranges from 2 to 14 days, and most infections (over 80%) show mild or no clinical symptoms of the disease (Ngonghala et al., 2020b). The common symptoms of the disease include fever, coughing and shortness of breath for mild cases, and pneumonia for severe cases. Although data clearly shows that most of the COVID-19 related deaths and severe cases typically occur in the elderly (i.e., people 65 years of age and older) and people with co-morbidities, such as people with diabetes, hypertension, obesity, kidney disease and other conditions that suppress or compromise the immune system, younger people and frontline healthcare workers are also at high risk of acquiring COVID-19 (Ngonghala et al., 2020b).

Coronaviruses (CoVs) are a major group of RNA viruses that cause diseases in mammals and birds. In humans, these viruses are associated with multiple respiratory diseases of varying severity. For instance, the mild form of coronavirus infections causes diseases such as the common cold, while the severe form can cause diseases such as the severe acute respiratory syndrome (SARS-CoV), middle eastern respiratory syndrome (MERS) and COVID-19 (caused by SARS-CoV-2). "Coronavirus" is derived from the Latin word "Corona", meaning crown or wreath, which is related to the characteristic appearance of the virions of the virus. Zoonotic scientists estimated that there are millions of coronaviruses in the wild, thereby making humans vulnerable to coronavirus pandemics periodically (since, owing to their genetic makeup, human coronaviruses are rated among the most rapidly evolving human viruses). It is believed that human coronaviruses have their origins in bats and rodents, and some human activities, such as urbanization and poultry farming, help in expediting their evolution.

Two pandemics of coronaviruses have occurred in recent years. These include the 2002/2003 pandemic of severe acute respiratory syndrome (SARS-CoV), a highly transmissible disease which started in the Guangdong province of China and spread to 29 countries (causing 8000 cases and 744 fatalities globally). Palm civet and bats were the natural reservoirs of SARS-CoV, which has a mortality rate of 10% (Li et al., 2005). In 2012, a pandemic of the middle eastern respiratory syndrome (MERS-CoV) started out of Saudi Arabia and spread to 27 countries, causing 2519 cases and 866 deaths by January 2020. Over 80% of MERS-CoV occurred in Saudi Arabia. MERS-CoV, which was believed to have originated from bats and then likely spread from infected dromedary (Arabian) camels to humans, has a mortality rate of about 35%. SARS-CoV and MERS-CoV have similar clinical symptoms. These include atypical pneumonia, marked by fever, headache and subsequent onset of respiratory symptoms (such as cough and pneumonia), which may lead to life-threatening respiratory failure and acute respiratory syndrome (Table 1 provides a detailed comparison of the aforementioned human coronavirus pandemics).

Although some promising anti-COVID-19 vaccines and antivirals are undergoing various stages of clinical trials (Iboi, Ngonghala, & Gumel, 2020), there is currently no safe and effective vaccine that has been approved for use in humans. Further, there are only very limited number of antivirals for use in humans, such as *remdesivir* (which is limited to individuals in hospital with severe symptoms of COVID-19). Consequently, control and mitigation efforts against COVID-19 are focused on the implementation of non-pharmaceutical interventions (NPIs), such as community lockdown, maintaining social (physical)-distancing, using face masks in public, quarantine of suspected cases, isolation and hospitalization of confirmed cases, surveillance and serology testing and contact tracing. This study introduces some of the basic principles and methodologies for using mathematical modeling, backed by rigorous analysis and statistical data analytics, to gain insight into the transmission dynamics and control of infectious diseases, such as COVID-19, in human populations.

A variety of mathematical model types, including statistical (e.g., Srivastava & Chowell, 2020), deterministic (e.g., Eikenberry et al., 2020; Iboi et al., 2020; Ngonghala et al., 2020a; Ngonghala et al., 2020b), stochastic (e.g., Hellewell et al.,

Table 1
Comparisons of human coronavirus pandemics: SARS-CoV, MERS-CoV and SARS-CoV-2 (COVID-19 data as of November 12, 2020).

	SARS-CoV	MERS-CoV	SARS-CoV-2 (COVID-19)
Origin	Guangdong, China	Jordan, Saudi Arabia	Wuhan, China
Duration	2002–2003	2012-to date	December 2019-to date
Reservoir	Bats and civet cats	Bats/camels	Bats (and possibly pangolins)
Countries affected	29	27	220
Incubation period	2–7 days	5 days	2–14 days
Confirmed global cases	8000	2519	52, 041, 441
Global mortality	744	866	>1, 282, 046
Case fatality ratio	9.5%	34.4%	2.5%

2020; Kucharski et al., 2020), network (e.g., Xue et al., 2020) and agent-based (e.g., Ferguson et al., 2020) models, have been used to study the transmission dynamics and control of COVID-19. A brief description of some of these modeling approaches is provided in Section 5. In this particular primer, we illustrate a basic modeling framework, based on using a simple Kermack-McKendrick-type compartmental (deterministic) epidemic model in a homogeneously-mixed population, for gaining insight into the transmission dynamics of COVID-19. The basic model will be used to assess the community-wide impact of some non-pharmaceutical and pharmaceutical intervention strategies, such as the use of face masks in public and social/physical-distancing. The basic modeling framework will be further extended to account for heterogeneity in community contacts (i.e., we will consider the dynamics of the disease in a heterogeneously-mixed population), vital demographic dynamics (i.e., birth and death processes), and to assess the potential population-level impact of a hypothetical COVID-19 vaccine.

2. Basic compartmental epidemic model for COVID-19 transmission

To design the basic epidemic model for COVID-19, we let $N(t)$ be the total human population size in the community at time t. This population is sub-divided into the mutually-exclusive compartments of susceptible (i.e., people who are at risk of acquiring infection, but have not yet contracted the disease) $((S(t))$, exposed (i.e., newly-infected individuals who are incubating the disease) $(E(t))$, symptomatically-infectious (i.e., infectious people showing clinical symptoms of the disease) $(I_s(t))$, asymptomatically-infectious (i.e., infectious people showing no clinical symptoms of the disease) $(I_a(t))$, hospitalized $(I_h(t))$ and recovered $(R(t))$ individuals. For simplicity, the compartment I_h also contains COVID-19 infected individuals who are self-isolating. Thus, $N(t) = S(t) + E(t) + I_s(t) + I_a(t) + I_h(t) + R(t)$. A major feature of COVID-19 is that a large fraction of infections (possibly over 80%) is generated by infected individuals who do not show clinical symptoms of the disease (i.e., individuals in the I_a compartment cause the bulk of COVID-19 infections) (Ngonghala et al., 2020b). In other words, the overwhelming majority of COVID-19 infections is generated by people who do not even know that they have the infection. This makes the effort to control the disease more difficult. Unless these (asymptomatically-infectious) individuals are detected (perhaps *via* random diagnostic testing for COVID-19 or contact tracing of the contacts of confirmed cases) and rapidly isolated, they will continue to unknowingly be spreading the pandemic. A model for COVID-19 should, at the very least, incorporate this important feature of asymptomatic transmission.

The Kermack-McKendrick-type epidemic models are built based on a number of simplifying assumptions, such as (a) a homogeneously-mixed population (i.e., all individuals in the community are assumed to have equal probability of coming in contact with one another), (b) exponentially-distributed waiting time in each epidemiological compartment (Hethcote, 2000; Ngonghala et al., 2020a; Nishiura & Chowell, 2009) and (c) no human demographic processes (i.e., no migration, births or deaths due to causes other than the disease being modeled). The assumption of no human demographic processes (i.e., vital dynamics) stems from the fact that, for a novel disease, such as COVID-19 (where, at the time of introduction, no member of the community has immunity due to natural recovery from prior exposure to the disease or due to immunization), the time scale of the disease is much smaller than the demographic time scale (i.e., the average lifespan of humans in the affected community). For instance, the novel SARS-CoV of 2002/2003 circulated for about 9 months in the 29 SARS-affected countries (including Canada). This time duration is certainly much smaller than the human demographic time scale in the affected countries (for instance, the demographic time scale in Canada is about 80 years). Disease transmission models that do not incorporate demographic processes are called *epidemic models*. It is further assumed that recovery from COVID-19 induces natural protective immunity against future infection (*albeit* there is currently no sufficient data to quantify the level and duration of the protective natural immunity).

In order to formulate the basic epidemic model for COVID-19, it should be noted that infection occurs when a susceptible individual (i.e., someone in the S compartment) has an effective contact (i.e., close contact capable of leading to the acquisition of COVID-19) with an infectious individual in either the asymptomatic (I_a), symptomatic (I_s), or hospitalized (I_h) class (it should be stressed that the compartment I_h also contains COVID-infected individuals in self-isolation either at home or in hospital). Based on this fact (and noting the flow diagram in Fig. 1), the basic model for COVID-19 transmission dynamics in a community is given by the following deterministic system of nonlinear differential equations (where a dot represents differentiation with respect to time t):

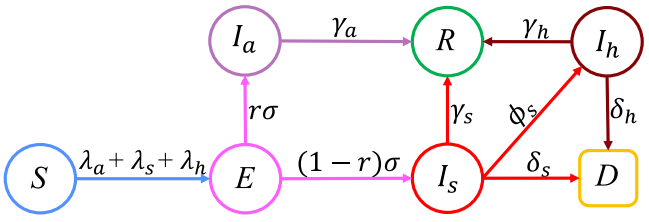

Fig. 1. Flow diagram of the model (1). Notation: $\lambda_a = \beta_a I_a/N$, $\lambda_s = \beta_s Is/N$, and $\lambda_h = \beta_h I_h/N$.

$$\begin{aligned}
\dot{S} &= - \frac{\beta_a I_a + \beta_s I_s + \beta_h I_h}{N} S, \\
\dot{E} &= \frac{\beta_a I_a + \beta_s I_s + \beta_h I_h}{N} S \quad \sigma E, \\
\dot{I}_a &= r\sigma E \quad \gamma_a I_a, \\
\dot{I}_s &= (1 \quad r)\sigma E - (\varphi_s + \gamma_s + \delta_s) I_s, \\
\dot{I}_h &= \varphi_s I_s - (\gamma_h + \delta_h) I_h, \\
\dot{R} &= \gamma_s I_s + \gamma_a I_a + \gamma_h I_h.
\end{aligned} \tag{1}$$

In (1), the parameters β_a, β_s and β_h represent, respectively, the rate at which asymptomatically-infectious, symptomatically-infectious, and hospitalized individuals transmit COVID-19 to susceptible individuals. It is assumed that $\beta_a \neq \beta_s \neq \beta_h$, to account for the possible heterogeneity in the contact rates of infectious individuals without clinical symptoms of COVID-19 (I_a), with clinical symptoms of COVID-19 (I_a) or with hospitalized individuals (I_h). For instance, it is reasonable to expect that asymptomatically-infectious humans have more contacts with members of the community than their symptomatic counterparts (because the former are less sick or not sick at all; hence, they can be expected to have more contacts, except if they abide by strict lockdown measures and stay at home). Exposed individuals progress out of the E class at a rate σ (i.e., $1/\sigma$ is the intrinsic incubation period of COVID-19). It is assumed that a proportion, $0 < r \quad 1$, of exposed individuals show no clinical symptoms of COVID-19 (and move to the I_a compartment) at the end of the incubation period. The remaining proportion, $1 \quad r$, show clinical symptoms and move to the I_s compartment at the end of the incubation period. Individuals in the $I_s(I_a)(I_h)$ compartment recover from COVID-19 infection at a rate $\gamma_s(\gamma_a)(\gamma_h)$. Infectious individuals are hospitalized (or isolated either at home or in hospital) at a rate φ_s. Individuals in the symptomatically-infectious (I_s) and hospitalized (I_h) compartments die of COVID-19 at a rate δ_s and δ_h, respectively. It is convenient, for housekeeping purposes, to consider the equation for the rate of change of the population of COVID-deceased individuals (denoted by $D(t)$) given by $\dot{D} = \delta_s I_s + \delta_h I_h$.

2.1. Asymptotic stability analysis of continuum of disease-free equilibria

The basic model (2.1) can be used to gain qualitative insight into the transmission dynamics of COVID-19 in a community, in addition to using it to assess the community-wide effectiveness of various control and mitigation strategies (such as the aforementioned NPIs and the potential use of an anti-COVID-19 vaccine). Before using the model to simulate the dynamics of the model and evaluate control strategies, it is instructive to explore its basic qualitative properties. The analysis of the model will be carried out in the following feasible region:

$$\Omega = \{(S, E, I_a, I_s, I_h, R) \in \mathbb{R}^6_+ : S + E + I_a + I_s + I_h + R \quad N(0)\}.$$

The region Ω is positively-invariant (i.e., solutions that start in Ω remain in Ω for all $t > 0$) and attracts all solutions of the model (2.1) (Ngonghala et al., 2020b). Hence, the model (1) is well-posed epidemiologically and mathematically in Ω (Hethcote, 2000).

We explore conditions for the local asymptotic stability of its associated steady-state solution(s) in the absence of disease. The model (2.1) has a continuum of disease-free equilibria (DFE), obtained by setting the right-hand sides of the equations for the rate of change of each of the state variables in (1) to zero, given by:

$$\mathcal{E}_0 = (S^*, E^*, I_s^*, I_a^*, I_h^*, R^*) = (N(0) - R^*, 0, 0, 0, 0, R^*),$$

where $N(0)$ is the initial total population size, $0 < S^* \quad N(0)$, $0 \quad R^* < N(0)$, and $0 < S^* + R^* \quad N(0)$. The linear asymptotic stability of the continuum of DFE can be explored using the *next generation operator method* (van den Driessche & Watmough, 2002; Diekmann, Heesterbeek, & Metz, 1990). To apply this method, it is convenient to consider the ordering (E, I_a, I_s, I_h) of the infected compartments of the model (1). The method entails computing two matrices, namely the non-negative matrix (F) of new infection terms near the continuum of DFE and the M matrix (V) of all the linear transmission terms associated with the model (1). Using the ordering (E, I_a, I_s, I_h), it can be seen that (where $N^* = S^* + R^*$)

$$F = \begin{bmatrix} 0 & \beta_a \frac{S^*}{N^*} & \beta_s \frac{S^*}{N^*} & \beta_h \frac{S^*}{N^*} \\ 0 & 0 & 0 & 0 \\ 0 & 0 & 0 & 0 \\ 0 & 0 & 0 & 0 \end{bmatrix} \text{ and } V = \begin{bmatrix} \sigma_1 & 0 & 0 & 0 \\ r\sigma & \gamma_a & 0 & 0 \\ -(1-r)\sigma_2 & 0 & \phi_s + \gamma_s + \delta_s & 0 \\ 0 & 0 & \phi_s & \gamma_h + \delta_h \end{bmatrix}$$

It follows that

$$\mathcal{R}_0 = \rho\left(FV^{-1}\right) = \mathcal{R}_a + \mathcal{R}_s + \mathcal{R}_h, \tag{2}$$

where,

$$\mathcal{R}_a = \frac{\beta_a r}{\gamma_a}\frac{S^*}{N^*}, \ \mathcal{R}_s = \frac{\beta_s (1-r)}{\varphi_s + \gamma_s + \delta_s}\frac{S^*}{N^*}, \ \mathcal{R}_h = \frac{\beta_h (1-r)\varphi_s}{(\varphi_s + \gamma_s + \delta_s)(\gamma_h + \delta_h)}\frac{S^*}{N^*} \tag{3}$$

The result below follows from Theorem 2 of (van den Driessche & Watmough, 2002).

Theorem 2.1. *The continuum of DFE* ($\mathcal{E}_0$) *of the model* (1) *is locally-asymptotically stable* (*LAS*) *if* $\mathcal{R}_0 < 1$. *If* $\mathcal{R}_0 > 1$, *the epidemic rises to a peak and then eventually declines to zero.*

The epidemiological implication of Theorem 2.1 is that a small influx of COVID-infected individuals will not generate an outbreak in the community if $\mathcal{R}_0 < 1$. That is, the disease rapidly dies out (when $\mathcal{R}_0 < 1$) if the initial number of infected individuals is in the basin of attraction of the continuum of the DFE ($\mathcal{E}_0$).

The quantity $\mathcal{R}_0$ is called the *basic reproduction number* of the model (1) (Kermack & McKendrick, 1927; Ngonghala et al., 2020b). It represents the average number of new COVID-19 cases generated by a typical infected individual introduced into a completely susceptible population (i.e., introduced into a population where no one has immunity due to prior infection or immunization, and no public health interventions are implemented in the community). In other words, $\mathcal{R}_0$ is a measure of the worst-case scenario where a disease is spreading in a community, and no public health control or mitigation measures are implemented. For instance, when $\mathcal{R}_0 = 2$, one infected individual will, on average, transmit COVID-19 to two others during the duration of his/her infectiousness (i.e., before he/she recovers or dies from the disease). Hence, in this scenario, the disease will be spreading rapidly (exponentially) until intervention and mitigation measures are implemented in the community and/or a certain proportion of the population becomes immune to the disease (following recovery from infection), thereby contributing to community-wide herd immunity (offering protection to the remaining susceptible population). When control and mitigation measures are implemented, another reproduction number, typically called the *control reproduction number* (and denoted by $\mathcal{R}_c$), is computed and used to study the dynamics of the model. In the presence of the control and mitigation measures, the total population consists of individuals who are completely susceptible (i.e., those in the S class), those who are infected and those who have developed some immunity (either due to recovery from prior infection or due to the implementation of public health interventions, such as vaccination, that reduces their susceptibility to acquisition of infection). Hence, when $\mathcal{R}_c = 2$, although one infected individual will infect, on average, two others in the community, the number of susceptible individuals available to this infected individual is reduced (due to the fact that some individuals in the community

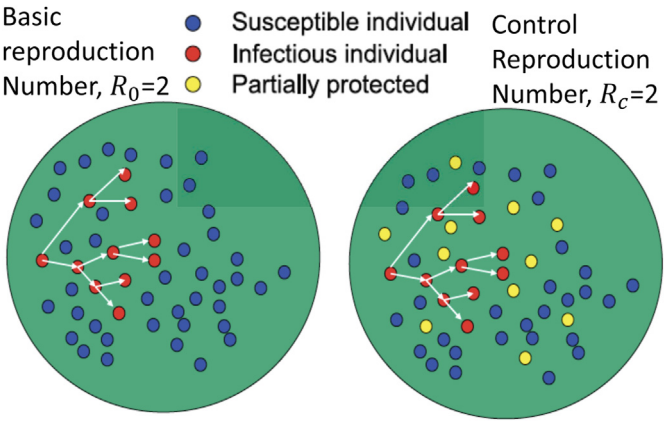

Fig. 2. Schematic illustrations of the basic reproduction number ($\mathcal{R}_0$) and the control reproduction number (denoted by $\mathcal{R}_c$).

are partially protected). Fig. 2 depicts a schematic illustration of the basic ($\mathcal{R}_0$) and control ($\mathcal{R}_c$) reproduction numbers of a generic disease transmission model, such as the model (1).

Remark 1. *It should be noted that the ratio $\frac{S^*}{N^*}$ can be simplified to $S^*/N^* = \frac{S^*}{S^*+R^*} = \frac{N(0)-R^*}{N(0)} = 1 \quad f_r$, where $0 \quad f_r = \frac{R^*}{N(0)} \quad 1$ is the proportion of individuals who recovered from, and are immune to, the disease). Then, it follows from Equations (2.2) and (2).3) (with S*/N* replaced by $1 \quad f_r$) that $\mathcal{R}_0$ decreases with increasing values of f_r, reducing to values near zero when $f_r \to 1$. In other words, the quantity $\mathcal{R}_0$ decreases with increasing levels of community-wide infection-acquired (natural) immunity (f_r). Thus, the higher the proportion of individuals with natural immunity, the higher the likelihood of eliminating the disease (as expected).*

The basic reproduction number ($\mathcal{R}_0$) of the model (1), given in (2) with (3), is expressed as the sum of the three constituent reproduction numbers, namely the reproduction number for the average number of new cases generated by symptomatically-infectious humans (denoted by $\mathcal{R}_s$), the average number of new cases generated by asymptomatically-infectious individuals ($\mathcal{R}_a$) and the average number of new cases generated by hospitalized/self-isolated individuals (denoted by $\mathcal{R}_h$). The terms in the constituent reproduction number $\mathcal{R}_s$ can be expressed as follows. They are the product of the infection rate of susceptible individuals by symptomatically-infectious humans, near the DFE ($\mathcal{E}_0$), given by $\beta_s \ \frac{S^*}{N^*}$, the proportion of exposed individuals that survived the incubation period and moved to the symptomatically-infectious class, given by $\frac{(1 \quad r)\sigma}{\sigma} = 1 \quad r$, and the average duration in the symptomatically-infectious class, given by $\frac{1}{\varphi_s+\gamma_s+\delta_s}$. Similarly, the terms in $\mathcal{R}_a$ are given by the product of the infection rate of susceptible humans with asymptomatically-infectious humans, near the DFE ($\mathcal{E}_0$), given by $\beta_a \frac{S^*}{N^*}$, the proportion that survived the exposed class (E) and moved to the asymptomatically-infectious class after the incubation period, given by ($\frac{r\sigma}{\sigma} = r$), and the average duration in the I_a class, given by $\frac{1}{\gamma_a}$. Also, the terms in $\mathcal{R}_h$ are given by the product of the infection rate of susceptible humans by hospitalized infectious humans, near the DFE ($\mathcal{E}_0$), given by $\beta_h \frac{S^*}{N^*}$, the flow rate (φ_s) from the symptomatically-infectious class (I_s) to the hospitalized class (I_h), and the average duration $\frac{1}{\varphi_s+\gamma_s+\delta_s}$ and $\frac{1}{\gamma_h+\delta_h}$ in the I_s and I_h classes, respectively. The sum of the terms in $\mathcal{R}_s$, $\mathcal{R}_a$ and $\mathcal{R}_h$ gives $\mathcal{R}_0$.

Remark 2. *The result of Theorem 2.1 can also be obtained by linearizing the model (1) around the continuum of DFE ($\mathcal{E}_0$) and requiring all six eigenvalues of the associated Jacobian matrix to have negative real parts.*

In order for disease elimination to be independent of the initial size of the sub-populations of the model (as required in Theorem 2.1), it is necessary to show that the continuum of disease-free equilibria ($\mathcal{E}_0$) is globally-asymptotically stable. We claim the following result:

Theorem 2.2. *The continuum of disease-free equilibria ($\mathcal{E}_0$) of the model (2.1) is globally-asymptotically stable in Ω if $\mathcal{R}_0 \quad 1$.*

Proof. The proof is based on using Lyapunov function (an energy-like function that decreases on trajectories). Consider the model (2.1) with $\mathcal{R}_0 < 1$. Furthermore, consider the following Lyapunov function:

$$\mathcal{L} = E + g_1 I_a + g_2 I_s + g_3 I_h, \text{ where } g_1 = \frac{\beta_a}{\gamma_a}, \ g_2 = \frac{\beta_s + g_3\varphi_s}{\varphi_s + \gamma_s + \delta_s}, \text{ and } g_3 = \frac{\beta_h}{\gamma_h + \delta_h}.$$

It follows that the Lyapunov derivative is given by:

$$\begin{aligned} \dot{\mathcal{L}} &= \dot{E} + g_1\dot{I}_a + g_2\dot{I}_s + g_3\dot{I}_h, \\ &= \beta_a\frac{I_a}{N}S + \beta_s\frac{I_s}{N}S + \beta_h\frac{I_h}{N}S \quad \sigma E \quad + g_1[r\sigma E \quad \gamma_a I_a] + \ g_2[(1 \quad r)\sigma E - (\ \varphi_s + \gamma_s + \delta_s)I_s] + \ g_3[\varphi_s I_s - (\ \gamma_h + \delta_h)I_h \ , \end{aligned}$$

which can be simplified to,

$$\begin{aligned} \dot{\mathcal{L}} &= \beta_a\frac{I_s}{N}S \quad g_1\gamma_a I_a \ + \ \beta_s\frac{I_s}{N}S + g_3\varphi_s \quad g_2(\varphi_s + \gamma_s + \delta_s)I_s \ + \ \beta_h\frac{I_h}{N}S \quad g_3(\gamma_h + \delta_h)I_h \\ &+ \quad \frac{r\beta_a\sigma}{\gamma_a} + \frac{(1 \quad r)\sigma\beta_s}{(\varphi_s + \gamma_s + \delta_s)} + \frac{(1 \quad r)\sigma\varphi_s\beta_h}{(\varphi_s + \gamma_s + \delta_s)(\gamma_h + \delta_h)} \quad \sigma \ E, \end{aligned}$$

so that (noting that $S(t) \quad N(t)$ for all t in Ω),

$$\dot{\mathcal{L}} \leq \sigma \frac{r\beta_a}{\gamma_a} + \frac{(1-r)\beta_s}{(\varphi_s+\gamma_s+\delta_s)} + \frac{(1-r)\varphi_s\beta_h}{(\varphi_s+\gamma_s+\delta_s)(\gamma_h+\delta_h)} - 1 \quad E,$$
$$\sigma(\mathcal{R}_0 - 1)E.$$

Hence, $\dot{\mathcal{L}} \leq 0$ if $\mathcal{R}_0 \leq 1$, and $\dot{\mathcal{L}} = 0$ if and only if $E(t) = 0$. Substituting $E(t) = 0$ in the model (1) shows that $(S(t), E(t), I_s(t), I_a(t), I_h(t), R(t)) \to (N(0), 0, 0, 0, 0, R^*)$, as $t \to \infty$. Furthermore, it can be shown that the largest compact invariant set in $\{(S(t), E(t), I_s(t), I_a(t), I_h(t), R(t)) \in \Omega : \dot{\mathcal{L}} = 0\}$ of disease-free equilibria ($\mathcal{E}_0$). Hence, it follows, by the LaSalle's Invariance Principle, that the continuum of disease-free equilibria of the model (1) is globally-asymptotically stable in Ω whenever $\mathcal{R}_0 \leq 1$. □

The epidemiological implication of Theorem 2.2 is that COVID-19 elimination is independent of the initial sizes of the sub-populations of the model (i.e., the initial number of infected individuals introduced into the community does not have to be within the basin of attraction of the disease-free equilibria, $\mathcal{E}_0$ of the model).

Effective Reproduction Number: Another useful threshold quantity in epidemiology is the time-varying *effective reproduction number*, denoted by $\mathcal{R}_c(t)$. For the model (1), $\mathcal{R}_c(t) = (\mathcal{R}_0)\left(\frac{S(t)}{N(t)}\right)$. The number of disease cases rises when $\mathcal{R}_c(t) > 1$, attains a peak when $\mathcal{R}_c(t) = 1$, and declines when $\mathcal{R}_c(t) < 1$ (Ngonghala et al., 2020a; Nishiura & Chowell, 2009). Fig. 3 depicts an illustration of the effective reproduction number for the basic model (1).

Remark 3. *It should be emphasized that for epidemic models (i.e., models with no demographic (births/deaths) processes), the disease always dies out, regardless of whether or not the associated reproduction number of the model is less, or greater, than unity (as shown in Theorems 2.1 and 2.2). However, for endemic models (i.e., disease transmission models that incorporate demographic (births and deaths) changes), the disease can only die out if the reproduction number of the model is less than unity (i.e., the disease persists if the reproduction number exceeds unity). This result can easily be shown using the next generation operator method (van den Driessche & Watmough, 2002; Diekmann et al., 1990) or standard linearization around the disease-free equilibrium of the endemic model.*

2.2. Computation of final size of the epidemic

For an ongoing epidemic, such as COVID-19, the *final size relation* (also known as the final size of the epidemic) provides useful qualitative insights into the dynamics of the epidemic (Arino, Brauer, van den Driessche, Watmough, & Wu, 2007; Brauer, 2017, 2019; Feng, 2007; Iboi et al., 2020; Ngonghala et al., 2020a, 2020b). Specifically, the final size relation provides an expression or inequality for the expected number of individuals in the community, who remain susceptible when the epidemic dies out in the community (thereby allowing for the estimate of the expected number of individuals in the community who acquired the infection during the course of the epidemic). Thus, final size relations can be used to assess the community-wide impact of various control and mitigation strategies implemented against the spread of the epidemic in the community.

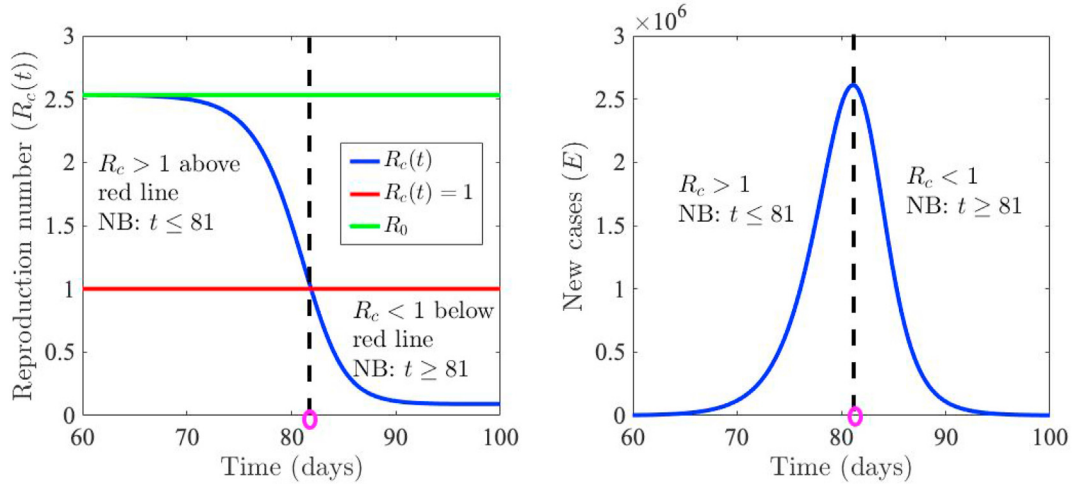

Fig. 3. (a) Time-varying effective reproduction number ($\mathcal{R}_c(t)$), as a function of time. (b) Simulation results of the basic model (2.1) illustrating sustained COVID-19 transmission when $\mathcal{R}_c(t) > 1$, and declining disease transmission (or disease incidence) when $\mathcal{R}_c(t) < 1$.

Numerous methods can be used to obtain the final size relation for an epidemic model, such as the basic model (1). Some of these methods are described in (Arino et al., 2007; Brauer, 2017, 2019; Feng, 2007). For the purpose of this study, the approach in (Arino et al., 2007) will be used. The general idea is to carry out some change of variables to reduce the basic model (1) into a three-dimensional system (for the rate of change of the susceptible, infected and recovered populations) and a next generation matrix to compute the basic reproduction number ($\mathcal{R}_0$) and, subsequently, the final size relation of the COVID-19 pandemic. In particular, following the notation in (Arino et al., 2007), it is convenient to let $x \in \mathbb{R}^4_+$, $y \in \mathrm{I}\,R_+$, and $z \in \mathrm{I}\,R_+$ represent the sets of infected, susceptible, and recovered components of the basic model (1). In other words, in relation to the state variables of the basic model (2.1), the transformed variable x is defined as $x(t) = (E(t), I_s(t), I_a(t), I_h(t))^T$. Similarly, $y(t) = S(t)$ and $z(t) = R(t)$. Let D be the $m \quad m$ diagonal matrix whose diagonal entries, denoted by $\sigma_i (i = 1, 2, \ldots, m)$, are the relative susceptibilities of the corresponding susceptible classes (Arino et al., 2007). Furthermore, let Π to be an $n \quad n$ matrix where the (i, j) entry of the matrix represents the fraction of the jth susceptible compartment that goes into the ith infected compartment upon becoming infected (Arino et al., 2007). Let b be an n dimensional row vector of relative horizontal transmissions. Further, in order to use the notation in (Arino et al., 2007), we use β for the infection rate of the basic model (1), λ. That is, $\lambda = \beta(x, y, z)$. Finally, we define the m dimensional vector $\Gamma = [\Gamma_1, \Gamma_2, \ldots, \Gamma_m] = \beta b V^{\ 1} \Pi D$ (Arino et al., 2007). It follows, by applying the above notation and definitions to the basic model (2.1), that:

$$m = 1,\ n = 4,\ b = [0, 1, 1, 1\ ,\ D \text{ is the scalar } 1,\ \text{and } \Pi = \begin{bmatrix} 1 \\ 0 \\ 0 \\ 0 \end{bmatrix} \Big($$

Hence, it follows, using the above change of variables and definitions, that the basic model (2.1) reduces to the following three-dimensional system:

$$\begin{aligned} \dot{x} &= \Pi D y \beta(x, y, z) b x \quad V x, \\ \dot{y} &= - D y \beta(x, y, z) b x, \\ \dot{z} &= W x, \end{aligned} \tag{4}$$

where W is a $k \quad n$ matrix with its (i, j) entry representing the rate at which individuals of the jth infected compartment transition into the recovered (ith z) compartment upon recovery and the matrix V is as defined in Section 2.1. Based on these transformations and definitions, Theorem 2.1 in (Arino et al., 2007) can be used to obtain the following expression for the basic reproduction number ($\mathcal{R}_0$, of the basic model (1) (or, equivalently, (4)): $\mathcal{R}_0 = \beta(0, y_0, z_0) b V^{\ 1} \Pi D y_0$ (which will be exactly the same as the expression we obtained in Equation (2) with (3)). Finally, Theorem 5.1 in (Arino et al., 2007) can be used to obtain the following result for the final size relation of the basic model (1) (or, equivalently, (4)).

Theorem 2.3. *Consider the basic model* (1) *and let* $S(\infty) = \lim_{t \to \infty} S(t)$. *The final size relation of the COVID-19 pandemic is given by*

$$\ln \frac{S(0)}{S(\infty)} \quad \frac{\mathcal{R}_0}{S(0)} [S(0) - S(\infty) + E(0)] + \frac{1}{S(0)} \frac{\beta_a}{\gamma_a} I_a(0) + \quad \beta_s + \frac{\varphi_s \beta_s}{\gamma_h + \delta_h} \quad \frac{I_s(0)}{\varphi_s + \gamma_s + \delta_s} \quad + \frac{\beta_h I_h(0)}{\gamma_h + \delta_h}$$

The implication of the above final size relation is that a bound can be placed on the number of people who remain susceptible at the end of the pandemic (by simply computing a bound on $S(\infty)$). Since the initial number of people susceptible to the disease ($S(0)$) is known before the introduction of the epidemic, a bound on the expected number of individuals who would become infected during the course of the epidemic can be obtained from the difference $S(0) \quad S(\infty)$. It is worth stating that, for the special case of the basic model (1) where the disease-induced mortality is negligible (e.g., $\delta_h = \delta_s = 0$), the inequality in Theorem 2.3 becomes equality (Brauer, 2019). Hence, for such special case (where, essentially, mass action incidence is used in the basic model (1), as against standard incidence for the infection rates), exact numbers (not just bounds) for the estimated final size of the COVID-19 pandemic can be computed. However, it should be mentioned that such assumption for negligible disease-induced mortality may not be realistic for diseases, such as COVID-19, that induce significant mortality in most populations.

2.3. Model fitting and parameter estimation

Before using the model to simulate COVID-19 scenarios in the US, and assess control and mitigation strategies, it is important to provide some measure of the reliability of the model. In particular, it is important to fit the model with observed data and use the fitting process to estimate parameters we do not have realistic estimates for. The model (1) contains 11 parameters. Realistic values for 7 of the 11 parameters are available in the literature. In particular, $\sigma = 1/5.1$ *per* day, $r = 0.48$, $\gamma_a = 1/5.1$ *per* day, $\gamma_s = 1/10$ *per* day, $\gamma_h = 1/8$ *per* day, $\delta_s = 0.015$ *per* day and $\delta_h = 0.04$ *per* day (Iboi et al., 2020; Ngonghala et al., 2020b). Additionally, we set and $f_r = 0$. The remaining five parameters, namely the community contact rate parameters

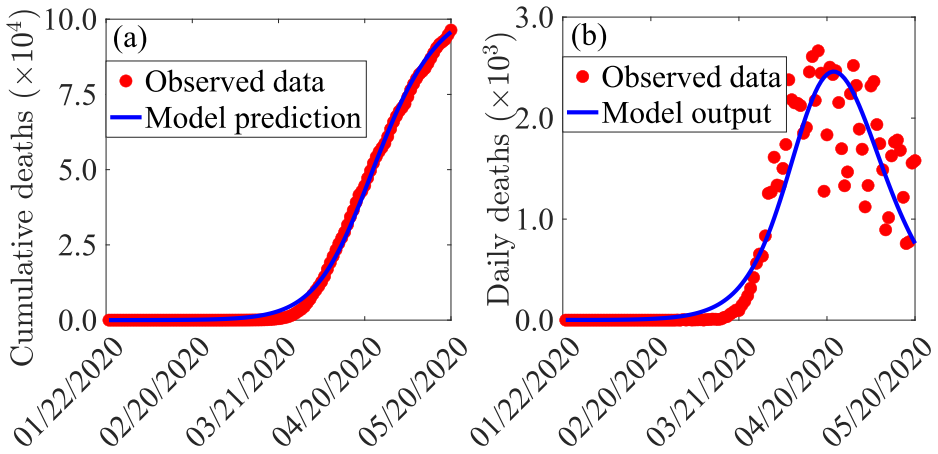

Fig. 4. (a) Data fitting of the model (1) using cumulative COVID-19 mortality data for the US from January 22 to May 20, 2020. (b) Simulations of the model (1) using the parameters estimated from the cumulative COVID-19 mortality data for the US.

(β_a, β_s, and β_h), the face mask compliance (c_m), and the hospitalization rate (φ_s) are obtained, by fitting the cumulative deaths profile generated from the model (2.1) (i.e., $\int_0^T D(t)dt$) to the observed COVID-19 cumulative mortality data for the US, using standard model fitting techniques, such as the least squares regression method (Banks, Davidian, Samuels, & Sutton, 2009, pp. 249–302; Chowell, 2017; Ngonghala et al., 2020b). The least squares regression method entails finding the best parameter regime that minimizes the root mean square difference between the predicted cumulative mortality generated from the (1) and the observed mortality data. The fitting for the model (2.1), using the COVID-19 cumulative mortality data for the US, is illustrated in Fig. 4 (a). We use the root mean square error (RMSE), where a smaller RMSE depicts a good fit as our measure of goodness of fit. The estimated parameter values and associated 95% confidence intervals for the unknown parameters obtained from the data fitting are $\beta_a = 0.7611$ ([0.3946, 0.8261]) *per* day, $\beta_s = 0.1925$ ([0.0556, 0.2929]) *per* day, $\beta_h = 0.0167$ ([0.0000, 0.1043]) *per* day, and $\varphi_s = 0.0221$ ([0.0127, 0.0279]) *per* day. For this set of parameter values (i.e., for the 7 known and 4 estimated parameters), the reproduction number of the model (2.1) is $\mathcal{R}_0 = 2.6544$ with 95% credible interval [1.1734, 3.1958] when $f_r = 0$. Furthermore, the curve for the daily mortality data plotted using the values of the 7 known parameters, together with the estimated values of the 4 unknown parameters, is depicted in Fig. 4 (b). It should be mentioned that, since the data used for fitting the model includes the periods when lockdown and face mask use strategies were implemented, the estimated parameters include some baseline (residual) level of lockdown and mask usage in the community.

2.4. Sensitivity analysis

The basic model (1) contains 11 parameters, and although some of the parameters were estimated using data, uncertainties are expected to arise in the estimates of some of the other parameters of the model. In models such as (1), it is crucial to measure the impact of the sensitivities of the parameters on the outcome of the numerical simulation results (with respect to a particular response function). We apply standard uncertainty and sensitivity analysis, using Latin Hypercube Sampling technique and partial rank correlation coefficients (PRCCs) (Marino, Hogue, Ray, & Kirschner, 2008; Blower & Dowlatabadi, 1994; McLeod, Brewster, Gumel, & Slonowsky, 2006), to determine the parameters of the model that have the most effect on the chosen response function. For illustration purposes, we choose the basic reproduction number of the basic model ($\mathcal{R}_0$) as the response function. The process of carrying out the sensitivity analysis entails defining a range (lower and upper bound) and distribution for each parameter of the model, and then splitting each parameter range into 1, 000 equal sub-intervals. Parameter sets are drawn from this space without replacement and used to form a $1,000 \times 11$ matrix. Each row of this matrix is used to compute the control reproduction number of the model ($\mathcal{R}_0$) and PRCCs are then computed to assess the contributions of uncertainty and variability in individual parameters to uncertainty and variability in the control reproduction number. Parameters with high PRCC values close to -1 or $+1$ are said to be highly correlated with the response function (those with negative(positive) PRCC values are said to be negatively (positively) correlated with the response function). We assume, for simplicity, that each of the 11 parameters of the model (2.1) obeys a uniform distribution, and the range for each parameter is obtained by taking 20% to the left, and then 20% to the right, of its baseline value (given in Section 2.3). The results obtained are depicted in Fig. 5. This figure shows that the parameters that have the most effect on the response function ($\mathcal{R}_0$) are the community contact rate by asymptomatically-infectious individuals (β_a), the proportion of exposed individuals who become asymptomatic after the incubation period (r), and the rate at which asymptomatic individuals recover from infection (γ_a). This result is consistent with the results reported in (Moghadas et al., 2020; Ngonghala

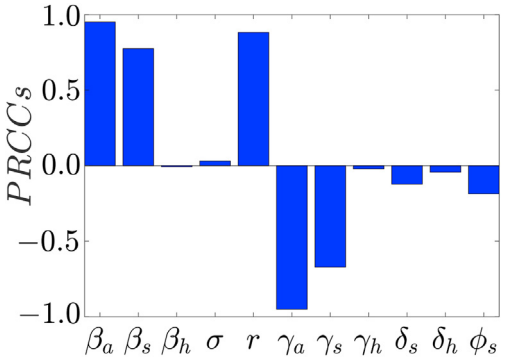

Fig. 5. Partial rank correlation coefficients (PRCCs) depicting the impact of model parameters on the control reproduction number ($\mathcal{R}_0$) of the model (1). The baseline values of the parameters are as given in Section 2.3.

et al., 2020a; Tindale et al., 2020), which suggest that pre-symptomatic and asymptomatic individuals are the main drivers of the COVID-19 pandemic. This figure shows that the community contact rate of symptomatically-infectious individuals (β_s) and the rate at which symptomatic individuals recover from infection (γ_s) also influence the control reproduction number significantly (*albeit* to a lesser extent, compared to the parameters associated with the asymptomatic population). Although we chose the basic reproduction number $\mathcal{R}_0$ as the response function, other metrics, such as the pandemic peak, total or cumulative number of hospitalized individuals, peak and total mortality and final epidemic size etc., can also be chosen as response functions.

2.5. Numerical simulations of basic model: assessment of control measures

Since the basic model (1) has been calibrated (i.e., the 11 parameters are properly estimated) and validated (by fitting it to the observed data in Section 2.3), the model can now be used to assess the various control and mitigation strategies against COVID-19 in the US. In particular, the model can be simulated to assess the community-wide impact of the various NPIs discussed earlier. In all the simulations we will discuss, the estimated values of the 11 parameters given in the parameter estimation section will be used (unless otherwise stated). The first set of simulations to be carried out is for assessing the potential community-wide impact of implementing a community lockdown strategy. In the context of this study, community lockdown entails implementing control and mitigation measures that target community transmission of COVID-19, such as stay-at-home, shelter-in-place, closures of school and non-essential businesses, cancelling large public gatherings and maintaining social-distancing (i.e., staying approximately 6 feet away from other humans) when in public. The model (1) can be slightly modified to allow for the assessment of the lockdown control measures. In particular, this is achieved by simply re-scaling the community contact rate parameters, β_a, β_s and β_h, to

$$\beta_a \to \beta_a(1 \quad \tilde{\epsilon}_l), \ \ \beta_s \to \beta_s(1 \quad \tilde{\epsilon}_l), \ \text{ and } \ \beta_h \to \beta_h(1 \quad \tilde{\epsilon}_l),$$

where $0 \quad \tilde{\epsilon}_l \quad 1$ is the effectiveness of lockdown (defined as the product of the efficacy of lockdown and the proportion of members of the community who adhere to (or comply with) the lockdown measures). Substituting the re-scaled expressions for β_a and β_s into the model (1), it can be shown (using the next generation operator method) that the control reproduction number of the modified version of the basic model (1) (denoted by $\mathcal{R}_{cl}$), which incorporates the implementation of a community lockdown strategy, is given by:

$$\mathcal{R}_{cl} = \frac{\beta_a(1 \quad \tilde{\epsilon}_l)\, r}{\gamma_a} + \frac{\beta_s(1 \quad \tilde{\epsilon}_l)\,(1 \quad r)}{\varphi_s + \gamma_s + \delta_s} + \frac{\beta_h(1 \quad \tilde{\epsilon}_l)\,\varphi_s\,(1 \quad r)}{(\varphi_s + \gamma_s + \delta_s)(\gamma_h + \delta_h)} = (1 \quad \tilde{\epsilon}_l)\mathcal{R}_0. \tag{5}$$

It can be seen from (5) that the control reproduction number ($\mathcal{R}_{cl}$) reduces to the basic reproduction number ($\mathcal{R}_0$) when lockdown and/or social distancing measures are not implemented in the community (i.e., when $\tilde{\epsilon}_l = 0$).

The use of face masks in public has historically been a major non-pharmaceutical intervention used to control the community transmission of respiratory diseases, such as COVID-19, dating back to the deadly 1918 H1N1 pandemic of influenza (Bootsma & Ferguson, 2007). Face masks play the dual role of preventing people who wear them from contracting respiratory infections, in addition to preventing those who are already infected from infecting others. The model (1) can easily be extended to allow for the assessment of the community-wide impact of the public face mask use strategy to combat COVID-19. Similar to the case for incorporating lockdown measures, public face masks use strategy can incorporated into the basic model (1) by re-scaling the community contact rate parameters, β_a, β_s and β_h, by a measure of face masks effectiveness. In particular, these parameters are now replaced by:

$$\beta_a \to \beta_a(1-\varepsilon_m c_m),\ \ \beta_s \to \beta_s(1-\varepsilon_m c_m),\ \ \text{and}\ \ \beta_h \to \beta_h(1-\varepsilon_m c_m),$$

where $0 \le \epsilon_m \le 1$ is the efficacy of the face mask and $0 \le c_m \le 1$ is the compliance in face masks usage in the community. It can be shown, by substituting the re-scaled expressions for β_a, β_s and β_h into the model (1), that the control reproduction number associated with the extended version of the model (1) that incorporates public face masks usage (denoted by $\mathcal{R}_{cm}$), is given by

$$\mathcal{R}_{cm} = \frac{\beta_a(1-\epsilon_m c_m)\, r}{\gamma_a} + \frac{\beta_s(1-\epsilon_m c_m)\,(1-r)}{\varphi_s+\gamma_s+\delta_s} + \frac{\varphi_s\beta_h(1-\epsilon_m c_m)\,(1-r)}{(\varphi_s+\gamma_s+\delta_s)(\gamma_h+\delta_h)} = (1-\epsilon_m c_m)\mathcal{R}_0. \tag{6}$$

Fig. 6 depicts the results obtained for simulating the modified version of the basic model (1) that incorporates lockdown measures. It shows that, starting from the index case in the US on January 22, 2020, the US records a daily COVID-19 mortality of about 2500 at the peak of the pandemic (Fig. 6 (a)) Furthermore, the model predicts up to 100, 150 cumulative deaths in the US by May 31, 2020 (Fig. 6 (b)). If the effectiveness of the lockdown measures is increased, as measured in terms of decrease in the values of the community contact rate parameters (β_a and β_s) of the modified version of the basic model (1) that incorporates community lockdown measures, the COVID-19 burden can be significantly reduced (as expected). For example, a 10% increase in the effectiveness of lockdown measures (i.e., a 10% reduction in the baseline values of the community contact parameters, β_a and β_s) will result in an 11% reduction in the cumulative deaths recorded in the US (Fig. 6 (b)). Further, a more stringent lockdown strategy that can reduce the baseline values of the community contact rate parameters by 40% will lead to a reduction of up to 96% of the cumulative deaths recorded in the US. More deaths will be averted if the lockdown measures were complemented with the use of face masks in public (Fig. 6 (b)). For example, a 20% increase in the effectiveness of lockdown measures combined with a 20% increase in face masks compliance (yellow curve in Fig. 6 (b)) will result in a 92%

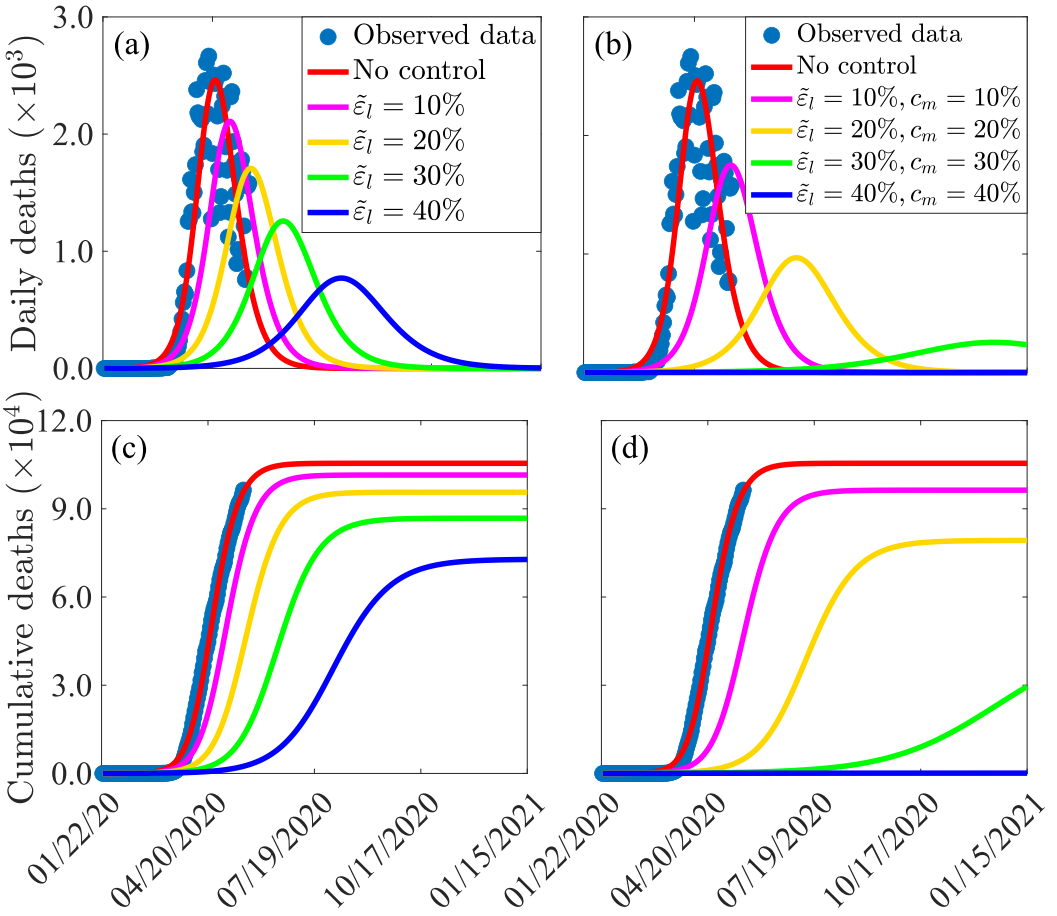

Fig. 6. Simulations of the extended version of model (2.1) allowing for the assessment of the impact of community lockdown strategy on COVID-19 (a) daily mortality and (b) cumulative mortality in the US. Additional simulations the extended version of model (2.1) allowing for the assessment of the combined impact of community lockdown and face mask use strategies on COVID-19 (a) daily mortality and (b) cumulative mortality in the US. Improvement in the effectiveness of the community lockdown and mask use strategies are measured in terms of a percentage reductions in the community contact rate parameters, β_a, β_s, and β_h, of the model. Parameter values used for the simulations are given in the parameter estimation section.

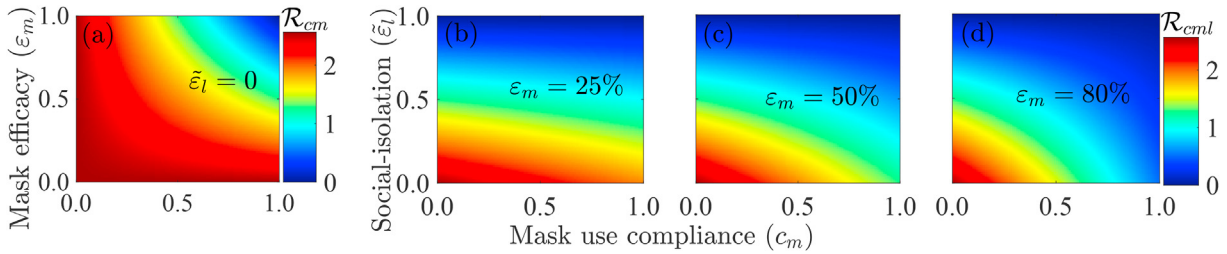

Fig. 7. (a) Heap map of the face mask reproduction number $\mathcal{R}_{cm}$, as a function of mask efficacy (ϵ_m) and compliance in mask use (c_m) when social-isolation (community lockdown/social distancing ($\tilde{\epsilon}_l$)) is at baseline (i.e., $\tilde{\epsilon}_l = 0$). (b)–(d) Heap maps of the face mask and social-isolation reproduction number $\mathcal{R}_{cml}$, as a function of $\tilde{\epsilon}_l$ and c_m for (b) $\epsilon_m = 0.25$, (c) $\epsilon_m = 0.5$, and (d) $\epsilon_m = 0.8$. The other parameter values used to generate the heat maps are as given in the parameter estimation section.

reduction in the cumulative number of deaths recorded in the US by May 31, 2020. These simulations show that implementing effective lockdown measures early and for a sustained period of time (such as implementing the lockdown measures nationwide from the January 22, 2020 date of the index case, and sustained until end of May 2020) would have significantly reduced the burden of COVID-19 mortality recorded in the US. In other words, this study emphasizes the fact that early implementation of effective control measures (and sustained for an optimal duration) can significantly curtail the burden of deadly respiratory diseases, such as COVID-19. This result is supported by the COVID-19 case data from Germany, Hong Kong, Japan, New Zealand, South Korea, Taiwan and Vietnam, showing the suppression of COVID-19 burden due to such timely and sustained efforts. It is worth stating that the pre-mature lifting of lockdown measures in May 2020 in the US resulted in a dramatic resurgence of COVID-19 in numerous US jurisdictions (see (Ngonghala et al., 2020a) for a detailed modeling study on whether or not the widespread use of face masks could halt such resurgence in the US). Finally, the effect of lockdown can also be assessed using more complex models, such as those that adopt a multi-group structure (i.e., models that stratify the total population in the community into those that adhere to lockdown measures and those that do not, in addition to allowing for back-and-forth transitions between the two groups, to account for human behaviour changes with respect to making the decision to adhere to lockdown measures or not). However, such complex models may not always give results that are not obtainable using single group models, such as (2.1). It should be mentioned that specific lockdown and re-opening periods implemented within specific US states or the entire US nation are not accounted for in these simulations. Partial lifting of the lockdown measures in the US (not accounted for here) resulted in a second COVID-19 wave that was bigger in size than the first wave. Thus, the mortality numbers depicted in Fig. 6 after May 2020 are lower than the actual recorded mortality (see (Ngonghala et al., 2020a) for a more comprehensive study on the impact of face mask usage on curtailing the post-lockdown resurgence of COVID-19 in some jurisdictions within the US and the entire US).

A heat map of the face mask reproduction number ($\mathcal{R}_{cm}$), as a function of face mask efficacy (ϵ_M) and compliance (c_M) for the case in which community lockdown/social distancing is maintained at baseline (i.e., $\tilde{\epsilon}_l = 0$), is depicted in Fig. 7 (a). This figure shows a decrease in the value of $\mathcal{R}_{cm}$ with increasing efficacy and compliance in face masks usage. That is, the use of face masks (even the low efficacy ones, such as the home-made cloths masks with estimated efficacy of 25% or less) will always reduce COVID-19 burden. Using highly efficacious face mask in the community, such as a face mask with efficacy of 88% (e.g., the N95 respirator), the simulations show that at least 69% nationwide compliance will be needed to bring $\mathcal{R}_{cm}$ to a value less than unity, needed to have a realistic chance to eliminate the pandemic (note that bringing the reproduction number of the model to a value less than unity is a necessary condition for the elimination of the disease, in line with Theorems 2.1 and 2.2). Such high compliance level is probably not realistically attainable in most communities. The prospects of COVID-19 elimination is greatly enhanced if the face masks strategy is combined with other community transmission reduction strategies (such as lockdown/social distancing) (Ngonghala et al., 2020b). For example, if lockdown and social-distancing measures could reduce community transmission by 55%, the use of low efficacy cloth masks (with efficacy of about 25%) can reduce the reproduction number of the model to a value less than unity if at least 57% of the population wears such mask in public (Fig. 7 (b)). The compliance level required to bring the reproduction number to a value below one, for this setting, if the more effective medical/surgical masks or even N95 respirators (with efficacy of at least 80%), reduces to only 28% (Fig. 7 (d)). As in the case of modeling the impact of community lockdown, the population-level impact of face mask use in public can be assessed using more complex models that, for instance, incorporate a multi-group structure based on face mask usage (as done in (Eikenberry et al., 2020)).

3. Extended epidemic model with heterogeneously-mixed populations

The basic epidemic model (1) was formulated based on the assumption that the population is homogeneous. That is, the population was assumed to be well-mixed, and each individual in the population is equally likely to mix with any other member of the population. However, SARS-Cov-2 transmission occurs in a diverse heterogeneous population. Hence, a more realistic approach is to divide the population into groups with similar characteristics, such as age, contact patterns, infectious period, or social, cultural, demographic, or geographic factors (Glasser, Feng, Moylan, Del Valle, & Castillo-Chavez, 2012). For

example, several mathematical models employ different mixing patterns, such as those between people of different age groups. These contact patterns are typically parametrized using empirical or synthetic social contact matrices estimated from population-based surveys (Mossong et al., 2008). Heterogeneity is captured here through differential contact rates and progression/recovery rates. To formulate the extended version of the model (1) with heterogeneous mixing, the total population at time t, denoted by $N(t)$, is divided into n distinct homogeneous groups or sub-populations (each with a total population of N_k, for $k = 1, 2, \ldots, n$). As in the formulation of the homogeneously-mixed model (1), each group is further divided into five mutually-exclusive compartments, namely susceptible (S), exposed (E), symptomatically-infectious (I_s), asymptomatically- infectious (I_a), hospitalized (I_h), and recovered (R). The heterogeneous-mixing model for COVID-19 dynamics consists of the following system of equations:

$$\begin{aligned}
\dot{S}_j &= -\lambda_j S_j,\\
\dot{E}_j &= \lambda_j S_j - \sigma_j E_j,\\
\dot{I}_{aj} &= r\sigma_j E_j - \gamma_{aj} I_{aj},\\
\dot{I}_{sj} &= (1-r)\sigma_j E_j - \varphi_{sj} + \gamma_{sj} + \delta_{sj}\ I_{sj},\\
\dot{I}_{hj} &= \varphi_{sj} I_{sj} - \gamma_{hj} + \delta_{hj}\ I_{hj},\\
\dot{R}_j &= \gamma_{sj} I_{sj} + \gamma_{aj} I_{aj} + \gamma_{hj} I_{hj},
\end{aligned} \tag{7}$$

where the associated *force of infection* is given by

$$\lambda_j(t) = \sum_{i}^{n} \sum_{k\in(s,a,h)} \left(\frac{c_{ji}\beta_k I_{ki}}{N_i}. \right. \tag{8}$$

In (8), β_k is the transmission probability *per* contact a susceptible individual makes with an infectious individual in category k (symptomatic (s), asymptomatic (a), or hospitalized (h)) and c_{ji} is the average number of contacts that an individual in group j has with individuals in group i during a certain period of time. Mixing should meet the following closure relation: $c_{ij}N_i = c_{ji}N_j$ (Glasser et al., 2012). For this model, we define $\dot{D}_j = \delta_{sj} I_{sj} + \delta_{hj} I_{hj}$.

3.1. Local asymptotic stability of continuum of disease-free equilibria: special case

We consider the heterogeneous mixing (3.1) with two groups (i.e., $n = 2$). For this special case, the basic reproduction number of the 2-group heterogeneously-mixed model, denoted by $\mathcal{R}_{0h}$, can be computed using the next generation operator method, with the associated new transmission matrix (F) and the matrix of linear transition terms (V) given, respectively, by:

$$F = \left[\begin{array}{cccccccc}
0 & 0 & \beta_s c_{11}\frac{S_1^*}{N_1^*} & \beta_s c_{12}\frac{S_1^*}{N_2^*} & \beta_a c_{11}\frac{S_1^*}{N_1^*} & \beta_a c_{12}\frac{S_1^*}{N_2^*} & \beta_h c_{11}\frac{S_1^*}{N_1^*} & \beta_h c_{12}\frac{S_1^*}{N_2^*}\\
0 & 0 & \beta_s c_{21}\frac{S_2^*}{N_1^*} & \beta_s c_{22}\frac{S_2^*}{N_2^*} & \beta_a c_{21}\frac{S_2^*}{N_1^*} & \beta_a c_{22}\frac{S_2^*}{N_2^*} & \beta_h c_{21}\frac{S_2^*}{N_1^*} & \beta_h c_{22}\frac{S_2^*}{N_2^*}\\
0 & 0 & 0 & 0 & 0 & 0 & 0 & 0\\
0 & 0 & 0 & 0 & 0 & 0 & 0 & 0\\
0 & 0 & 0 & 0 & 0 & 0 & 0 & 0\\
0 & 0 & 0 & 0 & 0 & 0 & 0 & 0\\
0 & 0 & 0 & 0 & 0 & 0 & 0 & 0\\
0 & 0 & 0 & 0 & 0 & 0 & 0 & 0
\end{array} \right],$$

and,

$$V = \left[\begin{array}{cccccccc}
\sigma_1 & 0 & 0 & 0 & 0 & 0 & 0 & 0\\
0 & \sigma_2 & 0 & 0 & 0 & 0 & 0 & 0\\
-(1-r)\sigma_1 & 0 & \phi_{s1}+\gamma_{s1}+\delta_{s1} & 0 & 0 & 0 & 0 & 0\\
0 & -(1-r)\sigma_2 & 0 & \phi_{s2}+\gamma_{s2}+\delta_{s2} & 0 & 0 & 0 & 0\\
-r\sigma_1 & 0 & 0 & 0 & \gamma_{a1} & 0 & 0 & 0\\
0 & -r\sigma_2 & 0 & 0 & 0 & \gamma_{a2} & 0 & 0\\
0 & 0 & -\phi_{s1} & 0 & 0 & 0 & \gamma_{h1}+\delta_{h1} & 0\\
0 & 0 & 0 & -\psi_{s2} & 0 & 0 & 0 & \gamma_{h2}+\delta_{h2}
\end{array} \right]$$

It follows that the basic reproduction number of the 2-group heterogeneously-mixed model is given by

$$\mathcal{R}_{0h} = \rho(FV^{-1}) = \frac{1}{2}\left(\Delta_1 + \sqrt{\Delta_1^2 - 4\Delta_2}\right), \tag{9}$$

where,

$$\begin{aligned} \Delta_1 &= \mathcal{R}_{a11} + \mathcal{R}_{a22} + \mathcal{R}_{h11} + \mathcal{R}_{h22} + \mathcal{R}_{s11} + \mathcal{R}_{s22}, \\ \Delta_2 &= (\mathcal{R}_{a11} + \mathcal{R}_{h11} + \mathcal{R}_{s11})(\mathcal{R}_{a22} + \mathcal{R}_{h22} + \mathcal{R}_{s22}) \\ &\quad -(\mathcal{R}_{a12} + \mathcal{R}_{h12} + \mathcal{R}_{s12})(\mathcal{R}_{a21} + \mathcal{R}_{h21} + \mathcal{R}_{s21}), \end{aligned} \tag{10}$$

with (noting that $i, j = 1, 2$),

$$\mathcal{R}_{sij} = \left[\frac{(1-r)c_{ij}\beta_s}{\gamma_{sj} + \delta_{sj} + \varphi_{sj}}\right]\left(\frac{S_i^*}{N_j^*}\right), \ \mathcal{R}_{aij} = \left[\frac{rc_{ij}\beta_a}{\gamma_{aj}}\right]\left(\frac{S_i^*}{N_j^*}\right), \ \mathcal{R}_{hij} = \left[\frac{(1-r)c_{ij}\beta_h\varphi_{sj}}{\gamma_{hj} + \delta_{hj}\quad \gamma_{sj} + \delta_{sj} + \varphi_{sj}}\right]\left(\frac{S_i^*}{N_j^*}\right)\left(\tag{11}$$

The result below follows from Theorem 2 of (van den Driessche & Watmough, 2002).

Theorem 3.1. *Consider the special case of the heterogeneous mixing model* (6) *with* n = 2. *The continuum of disease-free equilibria of this model is is locally-asymptotically stable if* $\mathcal{R}_{0h} < 1$. *If* $\mathcal{R}_{0h} > 1$, *the epidemic rises to a peak and eventually declines to zero.*

It should be mentioned that one of the simplest types of mixing is the separable proportionate mixing, in which the contacts of a person of group i are distributed over those of other groups in proportion to the activity levels and sizes of the other ages (Hethcote, 2000). Thus, under the proportionate mixing assumption, the following equation holds:

$$c_{ij} = \frac{c_i c_j}{\sum_{k=1}^{n} c_k N_k}, \tag{12}$$

where c_i is the average number of contacts an individual in group i makes *per* unit time. For this simplified version of the heterogeneous mixing model (6) (i.e., model (6) with proportionate mixing and with $n = 2$), it can be seen, by substituting (11) into (8) and simplifying, that the basic reproduction number of the model (6), $\mathcal{R}_{0h}$, reduces to $\mathcal{R}_{0hp} = \Delta_1$. Accounting for heterogeneities has important implications for determining the likelihood of an epidemic occurring and the final epidemic size and the magnitude of the interventions needed to stop an epidemic (see, for instance, (Clancy & Pearce, 2013; Cui, Zhang, & Feng, 2019)). However, analysis of disease transmission models in heterogeneous populations is more complex, and is often carried out using numerical methods (see, for instance, (Del Valle, Hyman, & Chitnis, 2013)).

4. Endemic model with vaccination

Vaccination is universally considered to be the best hope to effectively curtail (or eliminate) COVID-19 globally. Although there is currently no safe and effective vaccine for use in humans against COVID-19, a global (and expedited) concerted effort has been embarked upon aimed at developing such a vaccine. In particular, numerous promising anti-COVID-19 vaccines, such as those being developed at Oxford University or by Novavax and Mesoblast, are undergoing various stages of clinical trial (Iboi et al., 2020). Although vaccine development typically takes years, some of these efforts are expected to lead to a vaccine early next year. These vaccines are expected to offer some protective (but not perfect) efficacy against COVID-19 infection. It is, therefore, instructive to use mathematical models, such as (1), to assess the potential community-wide impact of a hypothetical anti-COVID-19 vaccine. Although several researchers expect the SARS-Cov-2 pandemic to end once herd immunity is reached (either through vaccination or naturally acquired), owing to its widespread and highly-transmissible nature, there is growing feeling that SARS-CoV-2 will become endemic, just like the other coronaviruses that cause the common cold. Thus, an endemic model, which allows for human demography (births/deaths processes) is more appropriate tool for accounting for these long-term outcomes.) Consequently, to assess the impact of such a vaccine on the dynamics of COVID-19, the model (1) will be extended to incorporate vital dynamics (births and deaths). Further, the susceptible population ($S(t)$) will be split into two sub-populations, namely the sub-population of unvaccinated susceptible (denoted by $S_u(t)$) and vaccinated susceptible ($S_v(t)$) individuals. It is assumed that the potential COVID-19 vaccine is imperfect, so that breakthrough infection (i.e., the infection of vaccinated susceptible individuals) can occur (but at a reduced rate, compared to the infection of unvaccinated susceptible individuals). It is also assumed that the vaccine-induced immunity may not last a lifetime. To incorporate a vaccine into the basic model (2.1), the first two equations are replaced by:

$$
\begin{aligned}
\dot{S}_u &= \Lambda + \omega_v S_v \quad \frac{\beta_s I_s + \beta_a I_a + \beta_h I_h}{N} \; S_u - (\mu + \xi_v) S_u, \\
\dot{S}_v &= \xi_v S_u \; -(1 \quad \epsilon_v) \; \frac{\beta_s I_s + \beta_a I_a + \beta_h I_h}{N} \; S_v - (\mu + \omega_v) S_v, \\
\dot{E} &= \quad \frac{\beta_s I_s + \beta_a I_a + \beta_h I_h}{N} \; S_u + (1 \quad \epsilon_v) \; \frac{\beta_s I_s + \beta_a I_a + \beta_h I_h}{N} \; S_v - (\mu + \sigma) E, \\
\dot{I}_s &= (1 \quad r)\sigma E - (\mu + \varphi_s + \gamma_s + \delta_s) I_s, \\
\dot{I}_a &= r\sigma E - (\mu + \gamma_a) I_a, \\
\dot{I}_h &= \varphi_s I_s - (\mu + \gamma_h + \delta_h) I_h, \\
\dot{R} &= \gamma_s I_s + \gamma_a I_a + \gamma_h I_h \quad \mu R,
\end{aligned}
\tag{13}
$$

where β_h represent the rate at which hospitalized individuals transmit COVID-19 to susceptible individuals, ξ_v is the vaccination rate, $0 < \epsilon_v \quad 1$ is the vaccine efficacy to protect against breakthrough infection (in vaccinated susceptible individuals), and ω_v is rate of loss of vaccine-induced immunity. All other parameters in (13) are as defined before. It is assumed, for simplicity, that the imperfect vaccine does not wane during the chosen time duration for the model simulations. It is also assumed that vaccine-induced protection can wane at a constant rate. Hence, the vaccination model for COVID-19 is given by the model (1) with its first equations replaced by the three equations in (13). For numerical simulation purposes, the vaccine-related parameters, ξ_v and ϵ_v, are estimated to be $\xi_v = 0.0010$ *per* day and $\epsilon_v = 0.8$, respectively (Iboi et al., 2020).

4.1. Asymptotic stability of disease-free equilibrium

The vaccination model (13) has a unique disease-free equilibrium given by:

$$
\mathcal{E}_{0V} = (S_u^*, S_v^*, E^*, I_s^*, I_a^*, I_h^*, R^*) = \quad \frac{\Lambda(\mu + \omega_v)}{\mu(\mu + \xi_v + \omega_v)}, \; \frac{\Lambda \xi_v}{\mu(\mu + \xi + \omega_v)}, \; 0, \; 0, \; 0, 0, 0 \quad ,
$$

and it can be shown, using the next generation operator method, that the *vaccination reproduction number* of the model (4.1), denoted by $\mathcal{R}_{cv}$, is given by:

$$
\mathcal{R}_{cv} = \mathcal{R}_0 \quad 1 \quad \epsilon_v \frac{S_v^*}{N^*} \quad , \tag{14}
$$

where, $\frac{S_v^*}{N^*} = \frac{\xi_v}{\mu + \xi_v + \omega_v}$. The result below follows from Theorem 2 of (van den Driessche & Watmough, 2002).

Theorem 4.1. *The disease-free equilibrium of the vaccination model* (13), *given by* $\mathcal{E}_{0\ V}$, *is locally-asymptotically stable if* $\mathcal{R}_{cv} < 1$, *and unstable if* $\mathcal{R}_{cv} > 1$.

In the absence of vaccination, the threshold quantity $\mathcal{R}_{cv}$ reduces to the basic reproduction number ($\mathcal{R}_0$), given by:

$$
\mathcal{R}_0 = \mathcal{R}_{cv}|_{\xi_v = S_v^* = 0} = \frac{\sigma}{\mu + \sigma} \; \frac{r\beta_a}{\mu + \gamma_a} + \frac{(1 \quad r)\beta_s}{(\mu + \varphi_s + \gamma_s + \delta_s)} + \frac{(1 \quad r)\beta_h \varphi_s}{(\mu + \varphi_s + \gamma_s + \delta_s)(\mu + \gamma_h + \delta_h)} \tag{15}
$$

4.2. Existence of endemic equilibria

In this section, conditions for the existence of endemic equilibria (i.e., equilibria where the compartments for infected individuals are nonzero) of the model (13) is explored. It is convenient to define:

$$
\lambda(t) = \frac{\beta_s I_s(t) + \beta_a I_a(t) + \beta_h I_h(t)}{N(t)}. \tag{16}
$$

It can be shown, by substituting (16) into the model (13) at steady-state (and simplifying), that the endemic equilibria of the vaccination model satisfy the following quadratic:

$$
a_2 \lambda^2 + a_1 \lambda + a_0, \tag{17}
$$

where,

$$\begin{aligned} a_0 &= \mu(\mu+\sigma)(\mu+\gamma_a)(\mu+\gamma_h+\delta_h)(\mu+\gamma_s+\delta_s+\varphi_s)(\mu+\xi_v+\omega_v)(1-\mathcal{R}_{cv}),\\ a_1 &= (\mu+\gamma_a)\{[(\mu+\sigma)(\mu+\gamma_h+\delta_h)(\mu+\gamma_s+\delta_s+\varphi_s)-(1 \quad r)\sigma(\mu+\gamma_h+\delta_h)\delta_s+\delta_h\varphi_s\\ &\quad (\mu+\xi_v(1 \quad \epsilon_v)+\omega_v)-\mu(\mu+\sigma)(\mu+\gamma_h+\delta_h)(1 \quad \epsilon_v)(\mu+\gamma_s+\delta_s+\varphi_s)(\mathcal{R}_0 \quad 1)\}\\ a_2 &= (\mu+\gamma_a)(1 \quad \epsilon_v)\{\sigma[r\delta_s(\mu+\delta_h+\gamma_h)+\varphi_s(r\delta_h+\gamma_h)+\gamma_s(\delta_h+\gamma_h)]+\mu[\sigma(\varphi_s+\gamma_s)+\\ &\quad (\sigma+\gamma_h)(\sigma+\varphi_s+\delta_s+\gamma_s)+\mu(\mu+\sigma+\delta_h+\gamma_h+\varphi_s+\delta_s+\gamma_s)]\} \end{aligned} \tag{18}$$

The endemic equilibria of System (4.1) can then be obtained by solving for λ from (17) and substituting the results into the steady-state expressions obtained from (13). The quadratic equation (16) can be analyzed for the possibility of multiple endemic equilibria when $\mathcal{R}_{cv}<1$. It should be noted that the coefficient a_2 is always positive, and a_0 is negative if $\mathcal{R}_{cv}>1$. Hence, the result below follows from the quadratic (16) with (17).

Theorem 4.2. *The vaccination model* (4.1) *has:*

(i) *a unique endemic equilibrium if* $a_0<0 \Leftrightarrow \mathcal{R}_{cv}>1$;
(ii) *a unique endemic equilibrium if* $a_1<0$, *and* $a_0=0$ *or* $a_1^2 \quad 4a_0a_2 = 0$;
(iii) *two endemic equilibria if* $a_0>0$, $a_1<0$, *and* $a_1^2 \quad 4a_0a_2>0$;
(iv) *no endemic equilibrium otherwise*.

Case (i) of Theorem 4.2 shows that the model (4.1) has a unique endemic equilibrium whenever $\mathcal{R}_{cv}>1$. Furthermore, Case (iii) of Theorem 4.2 suggests the possibility of backward bifurcation, a dynamic phenomenon characterized by the co-existence of multiple stable equilibria (a DFE and an a stable endemic equilibrium) when the associated reproduction number of the model ($\mathcal{R}_{cv}$) is less than unity (Gumel, 2012). The epidemiological implication of the phenomenon of backward bifurcation is that the requirement $\mathcal{R}_{cv}<1$, while necessary, is not sufficient for disease elimination. In this case, disease elimination will depend upon the initial sizes of the sub-populations of the model (Gumel, 2012). To compute the backward bifurcation point of the vaccination model, when $\mathcal{R}_{cv}<1$, we set the discriminant $a_1^2 \quad 4a_0a_2 = 0$ and solve for the critical value of $\mathcal{R}_{cv}$ (denoted by $\mathcal{R}_{cv}^*$) given by

$$\mathcal{R}_{cv}^* = 1 \quad \frac{a_1^2}{4a_2\mu(\mu+\sigma)(\mu+\gamma_a)(\mu+\gamma_h+\delta_h)(\mu+\gamma_s+\delta_s+\varphi_s)(\mu+\xi_v+\omega_v)}, \tag{19}$$

from which it can be shown that backward bifurcation occurs for values of $\mathcal{R}_{cv}$ such that $\mathcal{R}_{cv}^*<\mathcal{R}_{cv}<1$. The presence of backward bifurcation in the transmission dynamics of a disease makes its control or elimination difficult, since the reproduction number of the model has to be reduced to be significantly below unity (i.e., to be outside the backward bifurcation region) to have the possibility of the unique disease-free equilibrium being globally-asymptotically stable (Gumel, 2012). We now explore scenarios where the backward bifurcation phenomenon can be removed from the vaccination model. It is convenient to define the positively-invariant region

$$\Omega_V = \{(S_u, S_v, E, I_s, I_a, I_h, R) \in \mathbb{R}_+^7 : S_u+S_v+E+I_s+I_a+I_h+R \quad \Lambda \Big/ \Big(\mu\}.$$

Consider a special case of the vaccination model (13) with a perfect vaccine (i.e., consider the model (13) with $\epsilon_v=1$). We claim the following result.

Theorem 4.3. *Consider the vaccination model* (13) *with* $\epsilon_v = 1$. *The unique disease-free equilibrium* ($\mathcal{E}_{0\ v}$) *of this special case of the vaccination model is globally-asymptotically stable in* Ω_V *if* $\mathcal{R}_{cv} \quad 1$.

Proof: The proof is based on using Lyapunov function (an energy-like function that decreases on trajectories). Consider the model (2.1) with $\mathcal{R}_{cv}<1$. Furthermore, consider the following Lyapunov function:

$$\mathcal{L} = E+g_1I_s+g_2I_a+g_3I_h, \text{ where } g_1 = \frac{\beta_s+g_3\varphi_s}{\mu+\varphi_s+\gamma_s+\delta_s}, \ g_2 = \frac{\beta_a}{\mu+\gamma_a}, \text{ and } g_3 = \frac{\beta_h}{\mu+\gamma_h+\delta_h},$$

with Lyapunov derivative given by:

$$\begin{aligned} \dot{\mathcal{L}} &= \dot{E}+g_1\dot{I}_s+g_2\dot{I}_a+g_3\dot{I}_h,\\ &= \beta_s\frac{I_s}{N}S_u+\beta_a\frac{I_a}{N}S_u+\beta_h\frac{I_h}{N}S_u-(\mu+\sigma)E \quad +g_1[(1 \quad r)\sigma E-(\varphi_s+\gamma_s+\delta_s)I_s\\ &+ g_2[r\sigma E-(\mu+\gamma_a)I_a]+ g_3[\varphi_sI_s-(\mu+\gamma_h+\delta_h)I_h, \end{aligned}$$

which can be simplified to,

$$\dot{\mathcal{L}} = \beta_s\frac{I_s}{N}S_u + g_3\varphi_s \quad g_2(\varphi_s+\gamma_s+\delta_s)I_s + \beta_a\frac{I_a}{N}S_u \quad g_1(\mu+\gamma_a)I_a + \beta_h\frac{I_h}{N}S_u \quad g_3(\mu+\gamma_h+\delta_h)I_h$$
$$+ \frac{r\beta_a\sigma}{(\mu+\gamma_a)} + \frac{(1 \quad r)\sigma\beta_s}{(\varphi_s+\gamma_s+\delta_s)} + \frac{(1 \quad r)\sigma\varphi_s\beta_h}{(\varphi_s+\gamma_s+\delta_s)(\mu+\gamma_h+\delta_h)} - (\mu+\sigma) \quad E,$$

so that (noting that $S_u(t) \quad N(t)$ for all t in Ω_V),

$$\dot{\mathcal{L}} \leq (\mu+\sigma) \quad \frac{\sigma}{(\mu+\sigma)} \quad \frac{r\beta_a}{(\mu+\gamma_a)} + \frac{(1 \quad r)\beta_s}{(\varphi_s+\gamma_s+\delta_s)} + \frac{(1 \quad r)\varphi_s\beta_h}{(\varphi_s+\gamma_s+\delta_s)(\mu+\gamma_h+\delta_h)} \quad 1 \quad E,$$
$$\leq (\quad \mu+\sigma)(\mathcal{R}_{cv} \quad 1)E.$$

Hence, $\dot{\mathcal{L}} \leq 0$ if $\mathcal{R}_{cv} \quad 1$, and $\dot{\mathcal{L}} = 0$ if and only if $E(t) = 0$. Substituting $E(t) = 0$ in the model (1) shows that $(S(t), E(t), I_s(t), I_a(t), I_h(t), R(t)) \to (N(0) \quad R^*, 0, 0, 0, 0, R^*)$, as $t \to \infty$. Further, it can be shown that the largest compact invariant set in $\{(S(t), E(t), I_s(t), I_a(t), I_h(t), R(t)) \in \Omega_V : \dot{\mathcal{L}} = 0\}$ of disease-free equilibria ($\mathcal{E}_{0\ V}$). Hence, it follows, by the LaSalle's Invariance Principle, that the continuum of disease-free equilibria of the model (1) is globally-asymptotically stable in Ω_V whenever $\mathcal{R}_{cv} \quad 1$ □

Theorem 4.3 shows that the special case of the vaccination model (13) with perfect vaccine (i.e., $\epsilon_v = 1$) will not exhibit a backward bifurcation at $\mathcal{R}_{cv} = 1$. In other words, we show that the use of an imperfect vaccine (i.e., a COVID-19 vaccine with $0 < \epsilon_v < 1$) can cause the phenomenon of backward bifurcation in the transmission dynamics of COVID-19. Imperfect vaccine protection is known to induce backward bifurcation in disease transmission dynamics (see, for instance (Gumel, 2012),).

4.3. Herd immunity threshold

It should be mentioned that, for vaccine-preventable diseases, not all susceptible individuals can be immunized when a vaccine is available. For instance people with underlying health conditions, or females who are pregnant or people who opt out of vaccination for various reasons (traditional or other reasons) may not be vaccinated. In particular, vaccinating people in the first two categories may worsen their condition. The notion of *herd immunity* is used to determine the minimum proportion of the community-wide immunity that is needed to ensure that those that cannot be immunized can also be protected from acquiring infection. In other words, herd immunity is associated with the indirect protection members of a community receive when a large percentage of the population has become immune to the infectious disease due to natural recovery from prior infection or vaccination (Iboi et al., 2020). Sweden adopted the first option, of allowing people to acquire infection and (hopefully) recover. This has not proven to be successful to date. Vaccination remains the safest and fastest way to achieve herd immunity for vaccine-preventable diseases.

Let $f_v = S_v^*/N^*$ be the proportion of vaccinated susceptible individuals at the disease-free steady-state ($\mathcal{E}_{0V}$). To compute the herd immunity threshold associated with the vaccination model (4.1), we set the reproduction threshold, $\mathcal{R}_{cv}$, to one and solve for f_v. This gives

$$f_v = \frac{1}{\epsilon_v} \quad 1 \quad \frac{1}{\mathcal{R}_0} \quad = f_v^c. \tag{20}$$

It follows from (14) and (20) that $\mathcal{R}_{cv} < (>) 1$ if $f_v > (<) f_v^c$. Further, $\mathcal{R}_{cv} = 1$ whenever $f_v \quad = f_v^c$. This shows that vaccination will effectively control the pandemic if $f_v > f_v^c$ (i.e., if enough members of the community have been vaccinated to ensure $f_v > f_v^c$). Vaccination will not eliminate the disease if $f_v < f_v^c$ (the disease will persist in the population in this case). Theorem 4.3 can now be re-written in terms of the herd immunity threshold.

Theorem 4.4. *A perfect anti-COVID-19 vaccine (i.e., a vaccine with $\epsilon_v = 1$) can lead to the elimination of the pandemic if $f_v > f_v^c$ (i.e., if $\mathcal{R}_{cv} < 1$). If $f_v < f_v^c$ (i.e., if $\mathcal{R}_{cv} > 1$), then the disease will persist in the population.*

Using the parameter values given in the parameter estimation section, it can be seen from (4.4) that the vaccine-derived herd immunity threshold needed to combat COVID-19 in the US, using a vaccine with assumed efficacy of 80% (i.e., $\epsilon_v = 0.8$), is $f_v^c = 0.68$. Thus, at least 68% of the unvaccinated susceptible members of the US population need to be immunized in order to achieve herd immunity. Fig. 8 depicts a heat map of the vaccination reproduction number ($\mathcal{R}_{cv}$), as a function of vaccine efficacy (ϵ_v) and coverage at DFE (f_v), from which it can be seen that the vaccination reproduction number decreases with increasing vaccine efficacy and coverage. This figure shows that, based on the baseline values of the parameters of the model, eliminating COVID-19 using vaccination alone would require a vaccine with high efficacy and coverage (each nearly 70%). Achieving the required high vaccine coverage may not be realistically feasible. Hence vaccination program against COVID-19 would need to be supplemented with another intervention(s) to make the elimination of the pandemic more feasible in the US.

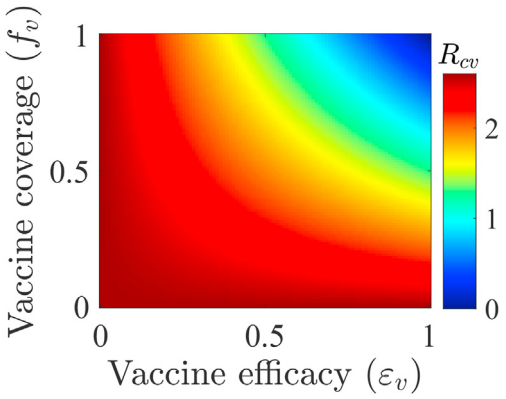

Fig. 8. Heat map of the vaccination reproduction number ($\mathcal{R}_{cv}$), as a function of vaccination coverage at the DFE, $\mathcal{E}_{0\ V}$ ($f_v = S_v^*/N^*$) and efficacy (ϵ_v). The other parameter values used to generate the heat map are as given in the parameter estimation section and $\mu = 3.4680 \quad 10^{-5}$.

5. Brief review of basic modeling types for infectious diseases

The literature on the use of mathematical modeling approaches to understand the spread and control of infectious diseases has a rich history, dating back to the pioneering works of Daniel Bernoulli (Bernoulli, 1760) and the modeling frameworks developed by Sir Ronald Ross (Ross, 1911) and Kermack-McKendrick in the early 1900s (Kermack & McKendrick, 1927). Although these pioneering works were based on using one modeling approach (compartmental modeling approach), numerous other modeling paradigms emerged out of these pioneering works. In general, mathematical models used to study the dynamics of infectious diseases fall into two broad categories, namely dynamic and statistical models. Dynamic models explore the evolution of disease processes over time and possibly space. Examples include deterministic, stochastic, network, and agent-based models. Many dynamic models are compartmental. That is, they are formulated based on splitting populations into mutually-exclusive compartments that represent disease status in the tradition of Kermack-McKendrick (Kermack & McKendrick, 1927). They are either continuous in time (continuous-time models) or discrete in time (discrete-time models). On the other hand, statistical models explore patterns and correlations in data using. For instance, statistical models use linear and/or mixed-effects regressions and time series analysis (Srivastava & Chowell, 2020; Tariq et al., 2020; IHME COVID-19 health service utilization forecasting team, 2020). We provide a brief review of dynamic models below.

5.1. Deterministic and stochastic models for infectious diseases

Deterministic models are also known as compartmental models, since they are formulated by subdividing the total population into sub-populations (known as compartments). These models describe what happens on average at the population scale, and do not account for the effect of randomness in the disease dynamics. Consequently, they produce the same outputs for the same parameter values and initial data. They are suitable for modeling large populations and they rely on the use of differential equations for continuous-time models and difference equations for discrete-time models. Stochastic models, on the other hand, are models in which the parameters and/or variables change randomly. They are used for smaller populations with higher transition rates or when demographic, and environmental variability impacts the epidemic outcome. Solutions or predictions from stochastic models are probability distributions for the random variables. Of the several stochastic epidemic models used in the study of infectious diseases, discrete-time Markov chain, continuous-time Markov chain, and the stochastic differential equations relate directly to their deterministic differential equation counterparts, but with properties that include the probability of an outbreak, the quasi-stationary probability distribution, the final size distribution of an epidemic and the expected duration of an epidemic (Allen, 2017). For large population sizes, the dynamics of stochastic models is similar to that of deterministic models. Numerous deterministic (Eikenberry et al., 2020; Iboi et al., 2020; Ngonghala et al., 2020a, 2020b) and stochastic (Hellewell et al., 2020; Hoertel et al., 2020; Kucharski et al., 2020) models have been used to study COVID-19 dynamics. Statistical models, such as those in (Srivastava & Chowell, 2020; Tariq et al., 2020; IHME COVID-19 health service utilization forecasting team, 2020), have also been used to study COVID-19 dynamics.

5.2. Network models

Network models are based on concepts from graph theory, where the nodes of a graph correspond to sub-populations, while the edges represent connections between the sub-populations. Connections between nodes can result in disease transmission on the network (Ming, Liu, Cheung, & Wan, 2016). Examples of network models include patch or meta-population, distance-transmission, and multi-group models. Network models can include a collection of deterministic or stochastic models for different sub-populations, which are connected in some way. Unlike in the case of simple deterministic

models, network models can easily become mathematically intractable. As such, some network models rely heavily on data and computer simulations. Network models are often used when the research question to be addressed involves heterogeneous populations that are connected through specific mechanisms. A number of network models, such as those in (Firth, Hellewell, Klepac, & Kissler, 2020; Thurner, Klimek, & Hanel, 2020; Xue et al., 2020), have been used to study the transmission dynamics and control of COVID-19.

5.3. Agent-based models

Agent-based models (also known as individual-based models) are computational models that are used to simulate the actions and interactions of autonomous agents (such as individuals or groups) with each other and with an environment. In other words, agent-based models are heterogeneous population models that explore interactions between individuals with different characteristics in order to understand the effects of the pathogen and these interactions on a population as a whole. A key feature of agent-based models is that the behavior or actions of agents are governed by a set of coded rules (and, at each time step, an agent decides its own action). Agent-based modeling formulation is often used when individual characteristics or characteristics of subgroups must be accounted for in the transmission dynamics of the disease being modeled. In agents-based models, computer simulations are used to study complex interactions between each individual in a social group and an epidemic disease. These models are obviously not mathematically-tractable. Hence, they rely heavily on data (i.e., they are *data hungry*) and are computationally-intensive. Ferguson et al. (Ferguson et al., 2020) developed and used an agent-based model to assess the impact of non-pharmaceutical interventions against COVID-19. Furthermore, agent-based models were used in (Cuevas, 2020; Hoertel et al., 2020) to study COVID-19 dynamics.

5.4. Choice of modeling type

The modeling types described above have been used to study the transmission dynamics and control of the 2019 novel coronavirus. For example, deterministic models were used in (Eikenberry et al., 2020; Ngonghala et al., 2020a, 2020b) to assess the impact of various NPIs on Covid-19. Hellewell et al. (Hellewell et al., 2020) used stochastic models to investigate the impact of contact-tracing and isolation on COVID-19. Similarly, Kucharski et al. (Kucharski et al., 2020) used a stochastic model to explore the path of COVID-19 in Wuhan, China. Ling Xue et al. (Xue et al., 2020) used a data-driven network model to study the dynamics of COVID-19 in Wuhan city of China, Toronto city in Canada, and Italy. Firth et al. (Firth et al., 2020) used a real-world network to assess localized COVID-19 control strategies. Ferguson et al. (Ferguson et al., 2020) used an agent-based model to assess the impact of non-pharmaceutical interventions against COVID-19. The Institute for Health Metrics and Evaluation (IHME) modeling team adopted a hybrid modeling approach, involving dynamic and statistical modeling, to project the burden of COVID-19 in the US (IHME COVID-19 health service utilization forecasting team, 2020). Srivastava and Chowell (Srivastava & Chowell, 2020) used statistical approaches to examine patterns in COVID-19 growth curves and to classify these curves based on their shapes and used this to assess the COVID-19 path in the US and among European countries. While some of the models used to understand COVID-19 have been theoretical, some have been data-driven (e.g., Tariq et al. (Tariq et al., 2020) used publicly-available data to estimate the time-varying (effective) reproduction number for COVID-19 dynamics in Singapore). In general, the choice of model type to use to study the dynamics of an infectious disease, such as COVID-19, depends on the specific modeling question(s) being asked and the availability (and quality) of data. In this particular paper, we describe our use of the Kermack-McKendrick deterministic modeling approaches to gain insight into the transmission dynamics of COVID-19 in the US.

Conclusions

We presented compartmental, deterministic models for gaining insight into the transmission dynamics and control of COVID-19 in the US. The first model, formulated as a basic Kermack-McKendrick epidemic model, has a continuum of disease-free equilibria which was shown to be locally- and globally-asymptotically stable whenever the associated basic reproduction number (denoted by $\mathcal{R}_0$) is less than unity. This provides a necessary condition for the elimination of the pandemic in the US. In addition to computing the final size of the pandemic (from which bounds can be placed on the total expected number of cases during the course of the pandemic), extensive numerical simulations were carried out to assess various non-pharmaceutical interventions (such as social distancing, community lockdown and face masks usage in public) implemented to control the spread of the disease. The basic epidemic model was extended to consider mixing within a heterogeneously-mixed population. The basic reproduction number of the extended epidemic model with heterogeneous mixing was also computed. An endemic model (i.e., a model with vital dynamics) was designed and used to assess the potential impact of a hypothetical (assumed to be imperfect) anti-COVID-19 vaccine in the US. Estimates for vaccine-derived community herd immunity, for various settings (based on community face masks compliance) were obtained. Simulations of the models we proposed suggest that the prospects of COVID-19 elimination in the US is promising using the aforementioned non-pharmaceutical interventions, particularly if they are implemented at high effectiveness and coverage levels, and in combinations. We also discussed and compared various types of models used to study COVID-19 dynamics, such as stochastic, agent-based and network models. Although the models we presented seem to be quite adequate in addressing the questions we studied (and, consequently, become adequate in capturing the observed dynamics of COVID-19 in the US), the

models can be extended in multiple ways to incorporate other aspects of COVID-19 dynamics. These include other types of heterogeneities, such as spatial, age and risk structure, in addition to adding social network structure and human behaviour (i.e., choices individuals make to interact with other individuals and their immediate environment). Furthermore, disease transmission by pre-symptomatic individuals can be accounted for (Ngonghala et al., 2020a). These suggested extensions will undoubtedly require more complexity in the formulation of the models (involving, for instance, using non-linear systems of partial differential equations and various model types, such as patch/metapopulation, social network and agent-based models). Further, the models we presented have numerous parameters, and uncertainties may arise in their estimated values. Hence, detailed uncertainty analysis can be carried out to assess the impact of such uncertainties in the numerical simulation results obtained to determine the parameters that have the highest effect on the chosen response function. The epidemiology of COVID-19 is undoubtedly complex, and realistically modeling it can pose serious challenges in terms of model formulation and the theoretical and statistical analysis of the models. We list a few of problems we consider to be important, challenging and currently open. The first challenge is to do with the fact that parameters related to the implementation of control measures should (realistically) be modeled as time-dependent, to account for the gradual refinement in, or improvement of, these control measures. The mathematical implication of doing so is that the resulting model becomes *non-autonomous*, and the theoretical analysis of such model, particularly if vital dynamics are incorporated into the model, is extremely challenging (requiring the development of new mathematical theory and methodology). Characterizing bifurcation types for such (non-autonomous) models is open. Another important problem associated with COVID-19 modeling is to do with fitting the models with observed data. COVID-19 models are typically large, and fitting them with the available case, mortality or hospitalization data often gives poor fittings because of the presence of numerous local minima (and standard model fitting software and methods are not robust enough to capture the associated global minimum, needed to achieve reliable fitting). This, together with addressing the important problem of identifiability (practical and structural) of models, constitute one of the most important and urgent problems associated with COVID-19 modeling. Another major open problem is, of course, the design of mathematical methods and theories for rigorously analysing compartmental models that account for the aforementioned heterogeneities (mixing, age structure, risk structure etc.). Some of the mathematical modeling challenges for COVID-19 dynamics include (i) designing realistic models for assessing the impact of school re-opening on COVID-19, (ii) modeling the potential impact of the flu season on COVID-19 and (iii) modeling optimal allocation of limited vaccine resources, (iv) modeling the impact of spatial heterogeneity on disease control (in particular, modeling the impact of effective control in one community and lack of such effective control in its neighbouring communities), and (v) using zoonotic data in the wild as a warning signal to predict the next coronavirus pandemic (epidemic intelligence).

Declaration of competing interest

None.

Acknowledgments

One of the authors (ABG) acknowledge the support, in part, of the Simons Foundation (Award #585022) and the National Science Foundation (Award #1917512). CNN acknowledges the support of the Simons Foundation (Award #627346). The authors are grateful to T. Malik (Merck Inc.) for useful editorial comments. The authors are grateful to the anonymous reviewers for their very constructive comments.

References

Allen, L. J. (2017). A primer on stochastic epidemic models: Formulation, numerical simulation, and analysis. *Infectious Disease Modelling, 2*, 128–142.
Arino, J., Brauer, F., van den Driessche, P., Watmough, J., & Wu, J. (2007). A final size relation for epidemic models. *Mathematical Biosciences and Engineering, 4*, 159.
Banks, H. T., Davidian, M., Samuels, J. R., & Sutton, K. L. (2009). *An inverse problem statistical methodology summary*. Dordrecht: Springer Netherlands (Online Version).
Bernoulli, D. (1760). Essai d'une nouvelle analyse de la mortalite causee par la petite verole, et des avantages de l'inoculation pour la prevenir. *Histoire de l'Acad., Roy. Sci.*, 1–45.
Blower, S. M., & Dowlatabadi, H. (1994). Sensitivity and uncertainty analysis of complex models of disease transmission: An HIV model, as an example. *International Statistical Review/Revue Internationale de Statistique, 62*, 229–243.
Bootsma, M. C., & Ferguson, N. M. (2007). The effect of public health measures on the 1918 influenza pandemic in US cities. *Proceedings of the National Academy of Sciences, 104*, 7588–7593.
Branswell, H. (2020). *WHO declares the coronavirus outbreak a pandemic*. Health (STATS) (Accessed on March 19, 2020)). Online Version.
Brauer, F. (2017). A final size relation for epidemic models of vector-transmitted diseases. *Infectious Disease Modelling, 2*, 12–20.
Brauer, F. (2019). The final size of a serious epidemic. *Bulletin of Mathematical Biology, 81*, 869–877.
Chowell, G. (2017). Fitting dynamic models to epidemic outbreaks with quantified uncertainty: A primer for parameter uncertainty, identifiability, and forecasts. *Infectious Disease Modelling, 2*, 379–398.
Clancy, D., & Pearce, C. J. (2013). The effect of population heterogeneities upon spread of infection. *Journal of Mathematical Biology, 67*, 963–987.
Cuevas, E. (2020). An agent-based model to evaluate the covid-19 transmission risks in facilities. *Computers in Biology and Medicine, 121*, 103827.
Cui, J., Zhang, Y., & Feng, Z. (2019). Influence of non-homogeneous mixing on final epidemic size in a meta-population model. *Journal of Biological Dynamics, 13*, 31–46.
Del Valle, S. Y., Hyman, J. M., & Chitnis, N. (2013). Mathematical models of contact patterns between age groups for predicting the spread of infectious diseases. *Mathematical Biosciences and Engineering, 10*, 1475.

Diekmann, O., Heesterbeek, J. A. P., & Metz, J. A. (1990). On the definition and the computation of the basic reproduction ratio R_0 in models for infectious diseases in heterogeneous populations. *Journal of Mathematical Biology, 28*, 365–382.
Dong, E., Du, H., & Gardner, L. (2020). An interactive web-based dashboard to track COVID-19 in real time. *The Lancet Infectious Diseases, 20*(5), 533–534.
van den Driessche, P., & Watmough, J. (2002). Reproduction numbers and sub-threshold endemic equilibria for compartmental models of disease transmission. *Mathematical Biosciences, 180*, 29–48.
Eikenberry, S. E., Muncuso, M., Iboi, E., Phan, T., Kostelich, E., Kuang, Y., et al. (2020). To mask or not to mask: Modeling the potential for face mask use by the general public to curtail the COVID-19 pandemic. *Infectious Disease Modeling, 5*, 293–308.
Feng, Z. (2007). Final and peak epidemic sizes for seir models with quarantine and isolation. *Mathematical Biosciences and Engineering, 4*, 675.
Ferguson, N. M., Laydon, D., Nedjati-Gilani, G., Imai, N., Ainslie, K., Baguelin, M., et al. (2020). *Impact of non-pharmaceutical interventions (NPIs) to reduce COVID-19 mortality and healthcare demand*. London: Imperial College COVID-19 Response Team. March 16.
Firth, J. A., Hellewell, J., Klepac, P., & Kissler, S. (2020). Using a real-world network to model localized covid-19 control strategies. *Nature Medicine*, 1–22 (Online Version).
Glasser, J., Feng, Z., Moylan, A., Del Valle, S., & Castillo-Chavez, C. (2012). Mixing in age-structured population models of infectious diseases. *Mathematical Biosciences, 235*, 1–7.
Gumel, A. (2012). Causes of backward bifurcations in some epidemiological models. *Journal of Mathematical Analysis and Applications, 395*, 355–365.
Hellewell, J., Abbott, S., Gimma, A., Bosse, N. I., Jarvis, C. I., Russell, T. W., et al. (2020). Feasibility of controlling COVID-19 outbreaks by isolation of cases and contacts. *The Lancet Global Health, 8*, E488–E496.
Hethcote, H. W. (2000). The mathematics of infectious diseases. *SIAM Review, 42*, 599–653.
Hoertel, N., Blachier, M., Blanco, C., Olfson, M., Massetti, M., Sanchez Rico, M., et al. (2020). A stochastic agent-based model of the sars-cov-2 epidemic in France. *Nature Medicine, 26*, 1417–1421.
Iboi, E. A., Ngonghala, C. N., & Gumel, A. B. (2020). Will an imperfect vaccine curtail the COVID-19 pandemic in the US? *Infectious Disease Modelling, 5*, 510–524.
IHME COVID-19 health service utilization forecasting team. (2020). *Forecasting COVID-19 impact on hospital bed-days, ICU-days, ventilator-days and deaths by us state in the next 4 months*. medRxiv.
Kermack, W. O., & McKendrick, A. G. (1927). A contribution to the mathematical theory of epidemics. In *Proceedings of the royal society of London. Series A, containing papers of a mathematical and physical character* (Vol. 115, pp. 700–721).
Kucharski, A. J., Russell, T. W., Diamond, C., Liu, Y., Edmunds, J., Funk, S., et al. (2020). Early dynamics of transmission and control of covid-19: A mathematical modelling study. *The Lancet Infectious Diseases, 20*, 553–558.
Li, W., Shi, Z., Yu, M., Ren, W., Smith, C., Epstein, J. H., et al. (2005). Bats are natural reservoirs of sars-like coronaviruses. *Science, 310*, 676–679.
Marino, S., Hogue, I. B., Ray, C. J., & Kirschner, D. E. (2008). A methodology for performing global uncertainty and sensitivity analysis in systems biology. *Journal of Theoretical Biology, 254*, 178–196.
McLeod, R. G., Brewster, J. F., Gumel, A. B., & Slonowsky, D. A. (2006). Sensitivity and uncertainty analyses for a SARS model with time-varying inputs and outputs. *Mathematical Biosciences and Engineering, 3*, 527–544.
Ming, R.-X., Liu, J., Cheung, W. K., & Wan, X. (2016). Stochastic modelling of infectious diseases for heterogeneous populations. *Infectious diseases of poverty, 5*, 1–11.
Moghadas, S. M., Fitzpatrick, M. C., Sah, P., Pandey, A., Shoukat, A., Singer, B. H., et al. (2020). The implications of silent transmission for the control of COVID-19 outbreaks. In *Proceedings of the national academy of sciences* (Online Version).
Mossong, J., Hens, N., Jit, M., Beutels, P., Auranen, K., Mikolajczyk, R., et al. (2008). Social contacts and mixing patterns relevant to the spread of infectious diseases. *PLoS Medicine, 5*, e74.
Ngonghala, C. N., Iboi, E., Eikenberry, S., Scotch, M., MacIntyre, C. R., Bonds, M. H., et al. (2020b). Mathematical assessment of the impact of non-pharmaceutical interventions on curtailing the 2019 novel coronavirus. *Mathematical Biosciences, 325*, 108364.
Ngonghala, C. N., Iboi, E., & Gumel, A. B. (2020a). Could masks curtail the post-lockdown resurgence of covid-19 in the US? *Mathematical Biosciences, 329*, 108452.
Nishiura, H., & Chowell, G. (2009). The effective reproduction number as a prelude to statistical estimation of time-dependent epidemic trends. In *Mathematical and statistical estimation approaches in epidemiology* (pp. 103–121). Springer.
Ross, R. (1911). *The prevention of malaria*. John Murray.
Srivastava, A., & Chowell, G. (2020). *Understanding spatial heterogeneity of COVID-19 pandemic using shape analysis of growth rate curves*. medRxiv.
Tariq, A., Lee, Y., Roosa, K., Blumberg, S., Yan, P., Ma, S., et al. (2020). Real-time monitoring the transmission potential of COVID-19 in Singapore, march 2020. *BMC Medicine, 18*, 1–14.
Thurner, S., Klimek, P., & Hanel, R. (2020). A network-based explanation of why most covid-19 infection curves are linear. *Proceedings of the National Academy of Sciences, 117*(37), 22684–22689.
Tindale, L. C., Stockdale, J. E., Coombe, M., Garlock, E. S., Lau, W. Y. V., Saraswat, M., et al. (2020). Evidence for transmission of COVID-19 prior to symptom onset. *eLife, 9*, Article e57149.
Xue, L., Jing, S., Miller, J. C., Sun, W., Li, H., Estrada-Franco, J. G., et al. (2020). A data-driven network model for the emerging covid-19 epidemics in Wuhan, Toronto and Italy. *Mathematical Biosciences, 326*, 108391.